JOURNAL OF GEOPHYSICAL RESEARCH, VOL. 108, NO. D14, 4420, doi:10.1029/2002JD002711, 2003

An investigation of cold cloud formation with a three-dimensional model with explicit microphysics

Elias Mavromatidis and George Kallos
School of Physics, Division of Applied Physics, University of Athens, Athens, Greece

Received 2 July 2002; revised 17 January 2003; accepted 26 February 2003; published 26 July 2003.

[1] In the framework of the European Union-funded project "Investigation of Cloud by Ground-based and Airborne Radar and Lidar" (CARL) the Regional Atmospheric Modeling System (RAMS) was used in order to study ice crystal formation and evolution in a cold cloud formation during a field program over Palaiseau, France. Sensitivity tests were performed so as to bind the uncertainty from various factors controlling model results. Emphasis is given to the sensitivity of the model with respect to the shape parameter of gamma distribution in the cloud microphysics module. Sensitivity analysis of the model was also performed in relation to the initialization of the simulation. The results are compared to in situ and remote sensing observations of the cloud formation. The analysis revealed that the model was able to reproduce the cloud characteristics (e.g., the spatial and temporal variability of the phenomena and the cloud geometry) in a satisfactory way. A detailed comparison of the model results with aircraft data showed that the model-calculated water content and number concentration deviate significantly for the small-size particle bin (2–47 microns) but are in good agreement for the medium- (25–800 microns) and large-size (200–6400 microns) bins. The differences for the smaller particles can partially be attributed to both poor performance of the microphysical algorithms and instrument inaccuracies. Some differences for the larger particles can be attributed either to the definition of the cloud boundaries by the model or to disturbances caused by the ascent path of the aircraft or both. The time of model initialization is also an important factor affecting cloud formation during the first few hours of the simulation. The performed simulations and model/data intercomparisons showed that RAMS is able to reproduce most of the microphysical parameters of cold cloud formations satisfactorily while utilizing conventional meteorological fields and observations for initial and boundary conditions. *INDEX TERMS:* 0320 Atmospheric Composition and Structure: Cloud physics and chemistry; 1863 Hydrology: Snow and ice (1827); 3329 Meteorology and Atmospheric Dynamics: Mesoscale meteorology; 3337 Meteorology and Atmospheric Dynamics: Numerical modeling and data assimilation; 3354 Meteorology and Atmospheric Dynamics: Precipitation (1854); *KEYWORDS:* cloud physics, numerical modeling, mesoscale phenomena, pristine ice, snow, radar

Citation: Mavromatidis, E., and G. Kallos, An investigation of cold cloud formation with a three-dimensional model with explicit microphysics, *J. Geophys. Res.*, *108*(D14), 4420, doi:10.1029/2002JD002711, 2003.

1. Introduction

[2] Upper tropospheric clouds, being characterized by temperatures of about −20 to −85°C, are referred to as cirriform clouds (cirrus, cirrostratus and cirrocumulus). It is widely considered that stratus, stratocumulus, altostratus, and cirrus clouds have the greatest impact on climate because of the large area they cover. Because of various ice crystal shapes, sizes, and concentrations, cirrus clouds play an important role in climate change [*Gultepe et al.*, 1995]. In particular, *Liou* [1986] stated that the knowledge of the global distribution of cirriform cloud properties is necessary to understand the role of ice clouds in climate. He pointed also that cirriform clouds primarily consist of ice particles. In addition, some convective elements may contain supercooled water. Airborne measurements of the composition of cirriform clouds showed values for ice contents in the range 0.001 to 0.25 g/m3 (typical values 0.01–0.1 g/m3), while the sizes of the particles range from 50 to 1000 microns [*Liou*, 1986]. The vertical component of the wind in these clouds is typically 0.1–0.2 m/s [*Gultepe and Heymsfield*, 1988].

[3] Recent studies increased our understanding of the size and shape of ice crystals in clouds, as well as of radiative transfer [*Stackhouse and Stephens*, 1991; *Kinne et al.*, 1992; *Fu and Liou*, 1993]. However, parameters such as size (effective diameter De), number (N_t) of droplets/crystals

0148-0227/03/2002JD002711$09.00

and liquid (or ice) water content (LWC/IWC) are strongly related to physical and dynamical structures within the clouds.

[4] The vertical distribution of liquid water content (LWC) and its relation to temperature (T) strongly affect the heat budget of the atmosphere. Because of the interest of climate/weather modelers regarding the LWC distribution in the vertical within clouds, *Gultepe and Isaac* [1997] used aircraft observations from several field projects to characterize the LWC-T relationship for northern latitudes. They suggested that the median LWC values increase monotonically with warmer temperatures. *Heymsfield* [1975, 1977] indicated the importance of dynamical processes on microphysics within stratiform and convective cirrus clouds. He suggested that the shape and number concentration of ice crystals in clouds are strongly affected by the vertical air velocity (w) and temperature (T). Larger vertical flow component (w) generates larger and more complicated ice crystals.

[5] In order to study cirrus cloud formation and development in depth, *Gultepe et al.* [1995] studied various dynamical structures including cells and turbulence during FIRE II project. Because of significant dynamic activity in the microscale (<1 km) and meso-γ-scale (<25 km) within cirrus, they have made scale separation at about 1 km. The results showed that dynamical processes, including coherent structures and small-scale turbulence, can play an important role in cloud development at scales less than 1 km. In another work, cloud dynamical structures and vertical air velocity were investigated by using aircraft, radar and LANDSAT observations during BASE field project [*Gultepe et al.*, 2000]. As it was stated, dynamical activity, representing vertical air velocity (w) and turbulent fluxes, is larger in cloud regions. *Gultepe et al.* [2000] also parameterized the ice crystal number concentration (N_t) from a heat budget equation and found that N_t is a function of vertical air velocity, radiative cooling, particle size and super-saturation.

[6] Until recently, the retrieval of cloud properties was achieved by using passive remote sensing measurements at the regional and global scale or by using in situ sensors at the local scale. New remote sensing instruments (e.g., combined radar and lidar systems) have been employed for more accurate information on cloud parameters, such as cloud boundaries or cloud microphysical properties, which are required for better cloud modeling (*Quante et al.* [2000] and *Fujiyoshi et al.* [1999], among others). Moreover, statistical relationships linking the measured signal to the cloud microphysical properties have been developed (*Matrosov* [1991], *Matrosov and Kropfli* [1993], *Matrosov et al.* [1994], *Sassen and Khvorostyanov* [1998], and *Platt et al.* [1998], among others). Recently, significant effort has been devoted to improving the current retrieval methods of cirrus properties by utilizing either multisensor approaches that combine passive and active instruments [*Miller et al.*, 2000], or by developing and testing cirrus cloud models with different physical schemes [*Starr et al.*, 2000].

[7] Weather prediction and climate models require accurate parameterizations for ice clouds in order to represent the complex radiation-cloud-atmospheric circulation feedbacks [e.g., *Jakob and Morcrette*, 1995; *Fowler and Randall*, 1996a, 1996b]. Errors in the initialization and parameterization techniques could change model results significantly, while successful modeling of clouds requires better understanding of various processes within the cloud. *Starr and Cox* [1985a, 1985b] used a 2-D nonhydrostatic model to study interactions between cloud physical-radiative development and dynamical changes. *Levkov et al.* [1992] evaluated cloud microphysical parameterizations within a 3-D nonhydrostatic mesoscale model, while cirrus development and forecasting over the Wisconsin area with the aid of a 2-D version of RAMS have been studied during FIRE project [*Heckman*, 1991; *Heckman and Cotton*, 1993]. In another work, *Kinne et al.* [1992] modeled radiative fluxes and compared the modeled values to measurements at various altitudes. Because of the importance of the shape and concentration of the small-size ice particles in the Earth's climate at the future [*Cooper*, 1991], *Kinne et al.* [1992] suggested that new aircraft instrumentation must be developed for the detection ice crystals with diameters ranging from 5 to 50 microns.

[8] In the present study the atmospheric model RAMS with explicit cloud microphysical scheme has been used to explore its capability and limitations for reproduction of cold cloud microphysical parameters. Specifically, the model performance and its capacity to be used in regular forecasting operations has been examined in order to obtain information on cloud formation and associated hydrometeors by utilizing conventional meteorological data for initial and lateral boundary conditions. For this reason, quantitative and qualitative definition of water content, number concentrations and diameters of the various water forms in the cloud have been made. Emphasis is given to the definition of the microphysical characteristics, which are sensitive to variations of the shape parameter ν of gamma distribution in the cloud microphysics module, as well as the initialization time of the simulation. The model results are compared to airborne, radar and lidar observations.

[9] The work performed is divided in sections as follows: Information about the experimental campaign, observations and an overview of the large-scale weather conditions occurred during the experimental period is presented in section 2. A general description of the model microphysical scheme is given in section 3, while section 4 describes the model setup. The model results are described and compared to the observations in section 5. In this section, the results of various model sensitivity tests are also included. Finally, the main results of the study are discussed and summarized in section 6.

2. Experimental Campaign, Observations, and Large-Scale Weather Conditions

2.1. Experimental Campaign

[10] During CARL project (Investigation of Cloud by Ground-based and Airborne Radar and Lidar) an experimental campaign was set up for the time period 26 April to 14 May 1999. The experiment was performed at the IPSL (Institut Pierre Simon Laplace) experimental site in Palaiseau, France, involving ground-based lidar-radar systems (see Table 1), as well as in situ validation measurements

Table 1. Characteristics of the Two Main Ground-Based Instruments

Device	Wavelength	Energy/Pulse	Pulse Frequency	Vertical Resolution	Field of View
Lidar Yag (IPSL)	0.532 μm	165 mJ	20 Hz	15 m	0.9 mrad
Cloud Doppler radar Miracle (GKSS)	3.2 mm-94.9 GHz	1.5 KW	50 Hz to 80 kHz	28 m	3 mrad

with the aid of the research aircraft ''Merlin'' from Meteo-France. The aircraft was carrying the GKSS cloud particle measuring system with three sizing probes for in situ microphysical measurements (see Table 2).

[11] The continuation of this effort was to make numerical simulations of the cloud field in order to asses the description of the meteorological conditions leading to the formation of the observed clouds, as well as the description of the cloud microphysical characteristics. The Regional Atmospheric Modeling System (RAMS), with full cloud microphysics, was applied to 4 May 1999 in order to derive the simulated cloud structure as a function of time. On this day the observations showed that cloud structure was slowly evolving, which favored comparisons with model simulations. Because of the latter, from cloud microphysics point of view this day was considered as the most interesting during the entire experimental period (3–7 May 1999). Details of the intensive experimental campaign and data collection systems and processing are given by *Pelon et al.* [2001].

2.2. Observations

[12] On 4 May the site located on the northeastern edge of a longwave trough with a cut-off system over southwestern Europe. The edge of a frontal cloud field was passing the site, while the radar detected from early morning a Ci/Ac cloud deck, varying in thickness. A homogeneous and deep Cs/As cloud formation within the layer 3.5–10 km was building up around 09:00 UTC (Figure 1a). This cloud formation, with maximum top up to 10.5 km, persisted for about six hours (until around 15:00 UTC) and was characterized by concentrations of ice particles. The corresponding Doppler velocity field, also measured by the radar, is shown in Figure 1b. According to *Pelon et al.* [2001], in the radar sections the height of the melting layer (about 2800 m) can be identified from the ''fallstreaks'' at about 08:00 UTC. In his description he noticed a sudden increase of the particle fall velocities below the melting layer, corresponding to a decrease in linear depolarization ratio (LDR) toward the value of cross polarization isolation (about −26 dB). As he explained, this sudden increase can be attributed to the change of the particle composition from irregularly shaped ice crystals to spherical water droplets, which have zero LDR and much higher fall speeds. During the same time period the lidar could penetrate only up to 4 km (Figure 2). However, the lidar data provide a more reliable cloud base (Figure 2) comparably to radar cloud bases (Figure 1). In this case the cloud bases provided by the radar are biased toward lower values because of large particles falling out of the altostratus [*Pelon et al.*, 2001].

2.3. Large-Scale Weather Conditions

[13] During the period 3–4 May 1999 the weather conditions over the area of interest, were characterized by intensive transport of air masses from North Africa toward the western Mediterranean Sea and the Italian Peninsula in the lower tropospheric layers.

[14] On 3 May the centers of action in the lower troposphere were a low-pressure system located over the Iberian Peninsula and the western Mediterranean, a second low-pressure system extending from Scandinavia to Siberia and, finally, an anticyclonic center located over the central Mediterranean and the Gulf of Syrtis. In the middle tropospheric layers a jet stream split was evident over the northeast Atlantic with one of its branches following the anticyclonic formation over England and the other toward the Iberian Peninsula and western Mediterranean curving sharply northward over France.

[15] This synoptic pattern resulted in the transport of continental-type air masses from Eastern Europe toward the experimental site in the lower troposphere (Figure 3a), while strong transport of maritime air masses was evident in the middle and upper troposphere (Figure 3c). Thin cirrus clouds started to appear over the experimental site at altitudes from 7 to 11 km, with dense patches at 13:30 up to 15:30 UTC (Figure 4).

[16] On the following day, the low-pressure system over southeast France moved to the east, toward the Gulf of Genoa, where it was intensified. This shift of the low resulted in the establishment of a strong southeasterly flow over France in the middle and upper troposphere, while in the lower troposphere the easterly flow shifted to northeasterly, causing the drop of temperature at the lower atmospheric levels and warming aloft (Figures 3a–3d). This warming caused a partial melting near the bottom cloud layers.

3. Model Description

[17] The analysis of the cloud layer is based on nested-grid simulations performed with RAMS model. RAMS is a well known numerical code developed at Colorado State University and the Aster Division of Mission Research Inc. (http://www.atmet.com) for simulating and forecasting meteorological phenomena [*Pielke et al.*, 1992]. It is based on a nonhydrostatic cloud model [*Tripoli and Cotton*, 1982] and a mesoscale model [*Mahrer and Pielke*, 1977]. The system allows simulation of the atmospheric processes on the scales of a few tens of meters to several thousand kilometers. A general description of the model and its capabilities are given by *Pielke et al.* [1992]. However,

Table 2. Ranges of Particle Sizes of the GKSS Probes

Instrument	Size Range
PMS FSSP-100	2–47 microns
OAP 2D2-C	25–800 microns
OAP 2D2-P	200–6400 microns

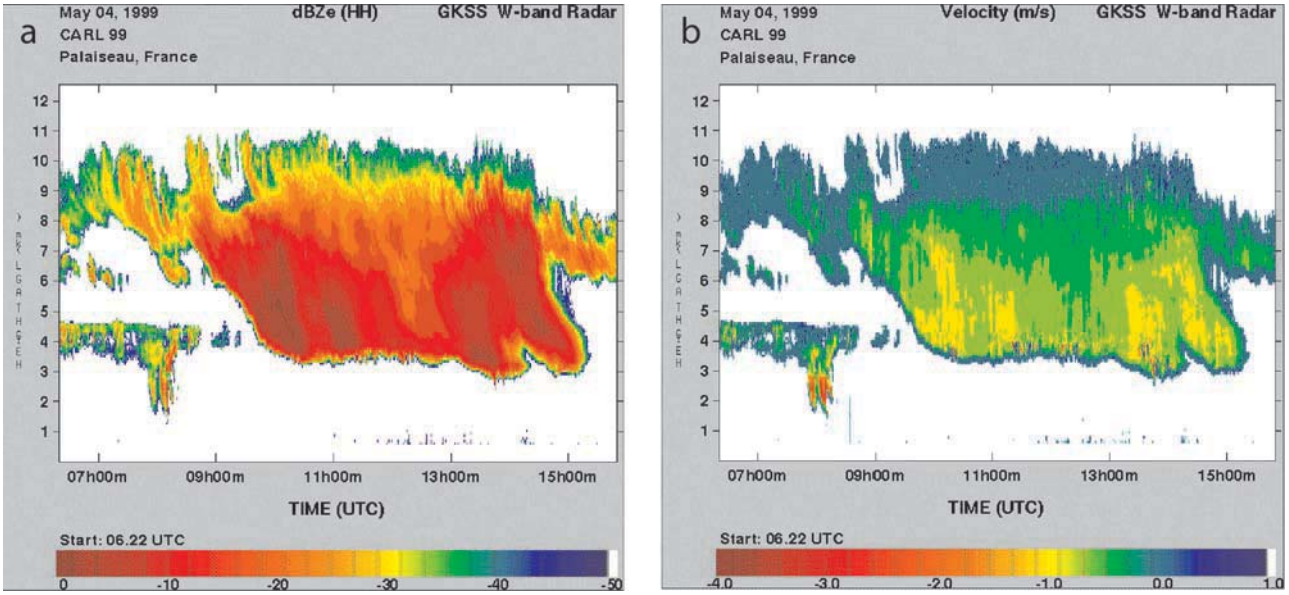

Figure 1. Time/height cross sections obtained from the GKSS 95 GHz cloud radar on 4 May 1999: (a) Radar reflectivity and (b) Doppler velocity [from *Pelon et al.*, 2001].

some of the RAMS feature can be summarized as follows: Two-way interactive nested grid structure [*Clark and Farley*, 1984]; terrain following coordinate surfaces; cloud microphysics parameterization; radiative transfer parameterizations (short and long wave); various options for upper and lateral boundary conditions; various levels of complexity for surface-layer parameterization.

[18] The RAMS model employs the single-moment scheme for parameterization of cloud microphysics [*Walko et al.*, 1995]. It introduces mixed phase hydrometeor cate-

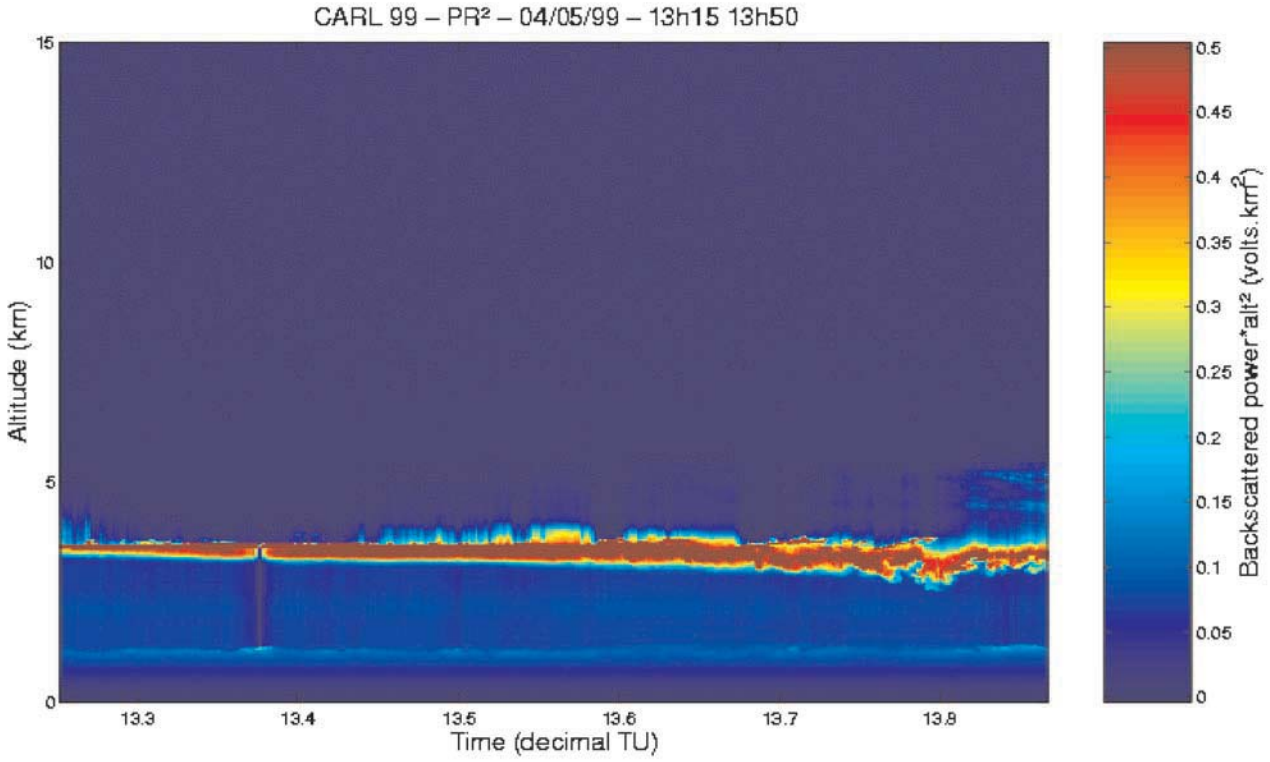

Figure 2. 532 nm Lidar backscatter power* alt^2 (Volts*km^2) measured on 4 May 1999 during the experimental campaign.

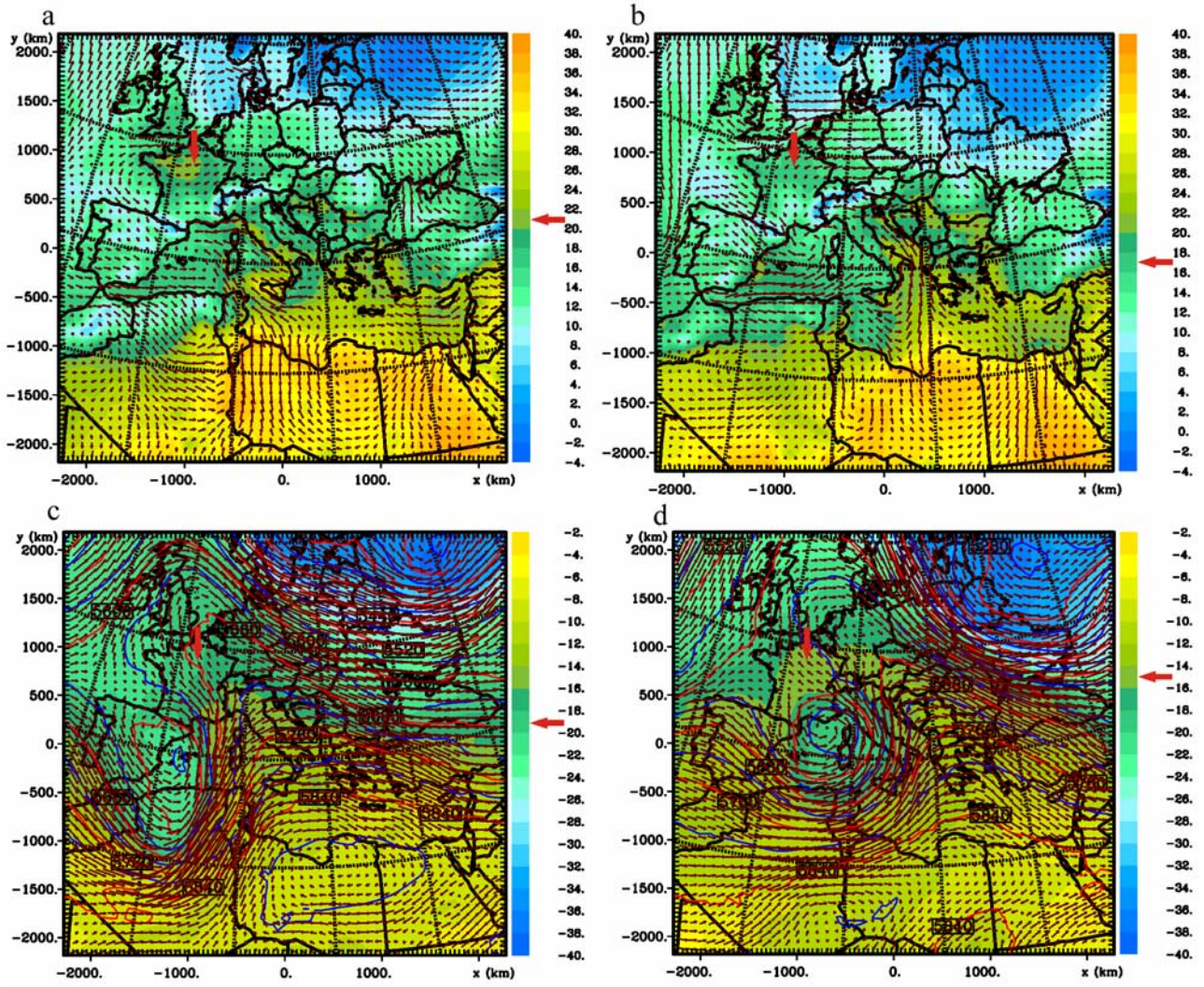

Figure 3. ECMWF analysis data. (a) Wind field (arrows) and temperature at the first level above the ground level (at 2°C intervals), for 12:00 UTC, 3 May 1999. (b) The same as Figure 3a but for 4 May 1999. (c) Geopotential height (at 40m intervals), temperature (at 2°C intervals) and wind field (arrows) at the 500 hPa isobaric surface, for 12:00 UTC, 3 May 1999. (d) The same as Figure 3c but for 4 May 1999. The big arrows are used as pointers to indicate the temperature drop at the lower atmospheric levels and the warming aloft.

gories (ice-liquid), a double moment spectrum for hydrometeors in ice form and a new sophisticated heterogeneous nucleation parameterization [*Harrington et al.*, 1995; *Meyers et al.*, 1997]. This explicit scheme includes equations for vapor, cloud water, rainwater, pristine ice, snow, aggregates, graupel and hail as well as warm rain conversion and accretion of cloud water to raindrops, evaporation and sedimentation. Nucleation of ice crystals, conversion nucleation and accretion of graupel, as well as ice crystal growth, evaporation, melting and sedimentation are also included. The initial concentration of cloud droplets, which will be activated, is specified as a climatologically derived input parameter.

[19] The cloud and raindroplets are water in the liquid phase. These two hydrometeor categories may be supercooled, while snow, aggregates and pristine ice are completely frozen. Graupel and hail are mixed-phase categories. They consist of a mixture of ice and liquid or ice only. All the categories can fall to the Earth, with the exception of cloud droplets and pristine ice, which are assumed too small to fall. Cloud droplets and pristine ice are the categories that nucleate from water vapor. All other hydrometeors build from existing hydrometeors, but once formed, may also grow by vapor deposition on their surface. Pristine ice particles are relatively small crystals and are not permitted to grow by any process other than vapor deposition. Larger pristine ice crystals are categorized as snow, which are relatively large ice crystals. These particles grow by vapor deposition and riming. Aggregates are formed by collision and coalescence of pristine ice, snow, and/or other aggregates. It is allowed for the aggregates to retain their identity with moderate amounts of riming. Graupel is assumed to be approximately spherical in shape and is forming by heavy riming and/or partial

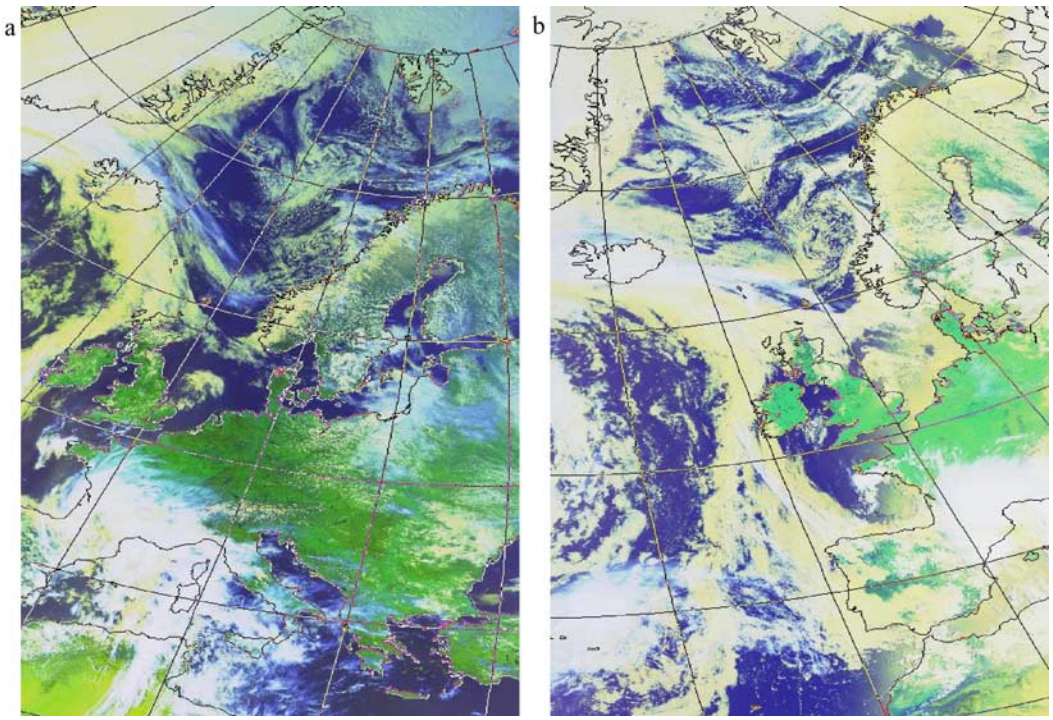

Figure 4. AVHRR image in channel 7 for (a) 13:56 UTC, 3 May 1999, and (b) 08:48 UTC, 3 May 1999.

melting of pristine ice, snow and aggregates. Graupel can only carry a small percentage of liquid. If this percentage is exceeded, the graupel is re-categorized as hail. Hail particles are considered spherical in shape. It is assumed that they are formed from freezing of raindroplets or by riming or partial melting of graupel. Hail is a high-density hydrometeor. Pristine ice, snow and aggregates are low-density ice particles with relatively low mass and fall speed for their diameters, while graupel is an intermediate density particle.

[20] It is assumed that hydrometeors in each category are distributed according to a generalized γ (gamma) function [*Flatau et al.*, 1989; *Verlinde et al.*, 1990]. The shape of the distribution is determined by a parameter (ν), which can be any real number greater than or equal to 1. This shape parameter controls the relative amount of smaller versus larger hydrometeors in the distribution. When $\nu = 1$, the exponential or Marshall-Palmer distribution is obtained, in which the number concentration decreases monotonically with the diameter throughout the size spectrum.

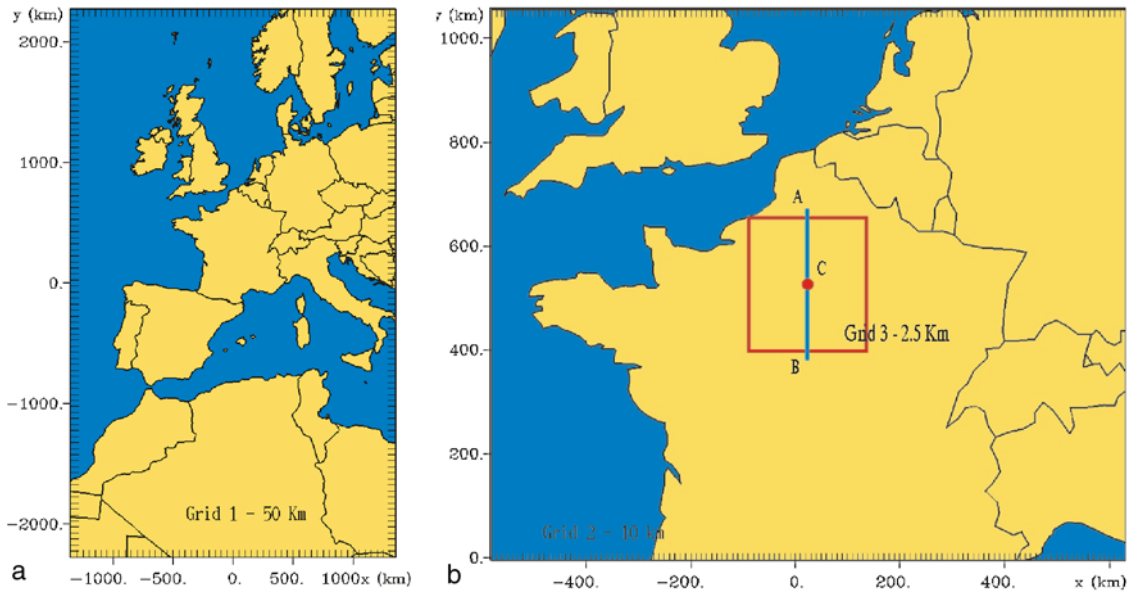

Figure 5. (a) Area covered from the first grid and (b) areas covered from the second and the third grind.

[21] The expression for the mass mixing ratio (mass of hydrometeor/mass of air) of any hydrometeor category is given by:

$$r = N_t a_m D_n^{\beta_m} \frac{\Gamma(\nu + \beta_m)}{\Gamma(\nu)}, \quad (1)$$

where the coefficient a_m is measured in kg/m$^{\beta m}$ (m is the mass of an individual hydrometeor (kg)), while the exponent β_m is dimensionless. In the same equation N_t (kg^{-1}) is the number concentration of a given hydrometeor category, $\Gamma(\nu)$ is a normalization constant and D_n is a characteristic diameter used to nondimensionalize the particle diameter D, and serves as a diameter scaling factor for the distribution.

[22] The prognostic equation of the mixing ratio (r) for the various hydrometeors, except for the cloud water and the vapor, includes terms for the advective and turbulent transport of r, terms which represent the possible generation or loss of the species r by microphysical processes and terms which account for local loss or gain of species r due to gravitational sedimentation. Prediction of the number concentration (N_t) is governed by a conservation equation of the same form as the equation of the mixing ratio.

4. Model Setup

[23] For the present application, the RAMS simulations were performed for the period 3–4 May 1999 (48 hours) on three nested grids in polar stereographic coordinates. Indeed, the computational domain of the model consisted of (1) the outer grid, with a mesh of 2700 × 4550 km (55 × 92 points) and 50 km horizontal resolution, centered at 44°N latitude and 2°15′E longitude (Figure 5a); (2) the second grid with a size of 1210 × 1060 km (122 × 107 points) and 10 km horizontal grid interval, centered at 48°44′N latitude and 2°15′E longitude (Figure 5b); and (3) the inner grid with a size of 232.5 × 262.5 km (94 × 106 points) and 2.5 km horizontal grid interval, centered at the same point with the second grid (Figure 5b).

[24] The center of the second and third grids coincides with the coordinates of the experimental site in Palaiseau. The top of the model domain is set at 18.3 km and the vertical atmospheric structure for the first grid is described by 45 model levels, which follow the topography. The first kinematic layer is at 46 m, while the grid stretching was 1.06 times the value of the first thermodynamic layer (95 m), with maximum spacing of 1000 m. Vertical nesting has been applied in the second and third grids, permitting adequate resolution of the cloud layer. For these grids (second and third), 51 vertical levels have been used. It should be noted that twenty (20) of these vertical layers have been defined within the lowest 2 km. Eight soil levels down to 0.6 m below the surface represent the soil layer, where heat and water variations are described.

[25] Since RAMS is in modular structure, the following model configuration options were used: (1) The Klemp/Wilhelmson [*Klemp and Wilhelmson*, 1978a, 1978b] radiative type lateral boundary conditions to the outer grid. (2) The convective dynamics are represented in the coarser grid by the Kuo-type cumulus parameterization scheme [*Kuo*, 1974] modified by *Tremback* [1990], while in all grids the explicit microphysics parameterization was activated. The shape parameter (ν) of the gamma distribution was set to be equal to 1 for all the hydrometeor categories. The concentration of activated cloud droplets were chosen to be equal to 0.3 × 10^9 (#/m^3), which is a climatologically derived value used in simulations for similar cases. Sensitivity tests with different initial concentrations of cloud droplets showed that the model establishes equilibrium within a period of less than 3 hours. This is due to the fact that all the hydrometeor categories are resolved explicitly in the microphysical scheme. (3) The radiation scheme developed by *Chen and Cotton* [1983], which takes into account the influence of water vapor and condensates on short wave, and long wave radiative transfer.

[26] Gridded fields of the European Centre for Medium-Range Weather Forecasts (ECMWF) objective analysis with 0.5° horizontal resolution determined on 12 isobaric surfaces (1000, 925, 850, 700, 500, 400, 350, 300, 250, 200, 100 and 50 hPa) were adapted as initial data. In addition, approximately 60 upper air soundings and more than 500 surface observations have been employed in 6-hour intervals in the data assimilation scheme of RAMS for preparation of the initial conditions. Average monthly sea-surface temperatures (SST) with 1° horizontal resolution were used for the water body. The topography used for all grids is based on an initial set with 30″ resolution (USGS data set). Finally, gridded vegetation type data of 30″ resolution was used to derive vegetation cover at each grid cell.

[27] This model setup is capable of covering a wide range of the spectrum of atmospheric disturbances ranging from synoptic to meso-γ scale. This is absolutely necessary because the factors controlling the cloud formation span this wide range. The Klemp/Wilhelmson condition for lateral boundary conditions was chosen because of the fact that this boundary condition allows most disturbances to propagate out of the model domain without strongly reflecting back into the interior. In this scheme the normal velocity component specified at the lateral boundary is effectively advected from the interior, assuming a propagation speed similar to a dominant gravity wave phase speed (for this study cphase = 20 m/s). The Chen and Cotton scheme was chosen for the longwave and shortwave radiation because of the fact that it is considered as the most appropriate for cloudy environments from the available in RAMS.

[28] The microphysics scheme in RAMS code activates the microphysical parameterization of rainwater, graupel, pristine ice, aggregates, hail and snow species. For each hydrometeor the model activates the prognostic equations for number concentration and mixing ratio. The hydrometeor diameters are diagnosed from the predicted mixing ratio and number concentration.

[29] Because of the importance of the model domain characteristics (e.g., domain size, vertical layering), the vertical structure of the inner RAMS grid was emphasized for a satisfactory vertical representation of the atmospheric layering. The area covered by the coarse grid was defined in such a way in order to better simulate the current atmospheric synoptic flow that influenced the greater area of interest. Both definitions were made so as to have a reasonable computational load.

[30] The aforementioned setup constitutes the control run (N1 hereafter). In order to test the role of shape parameter

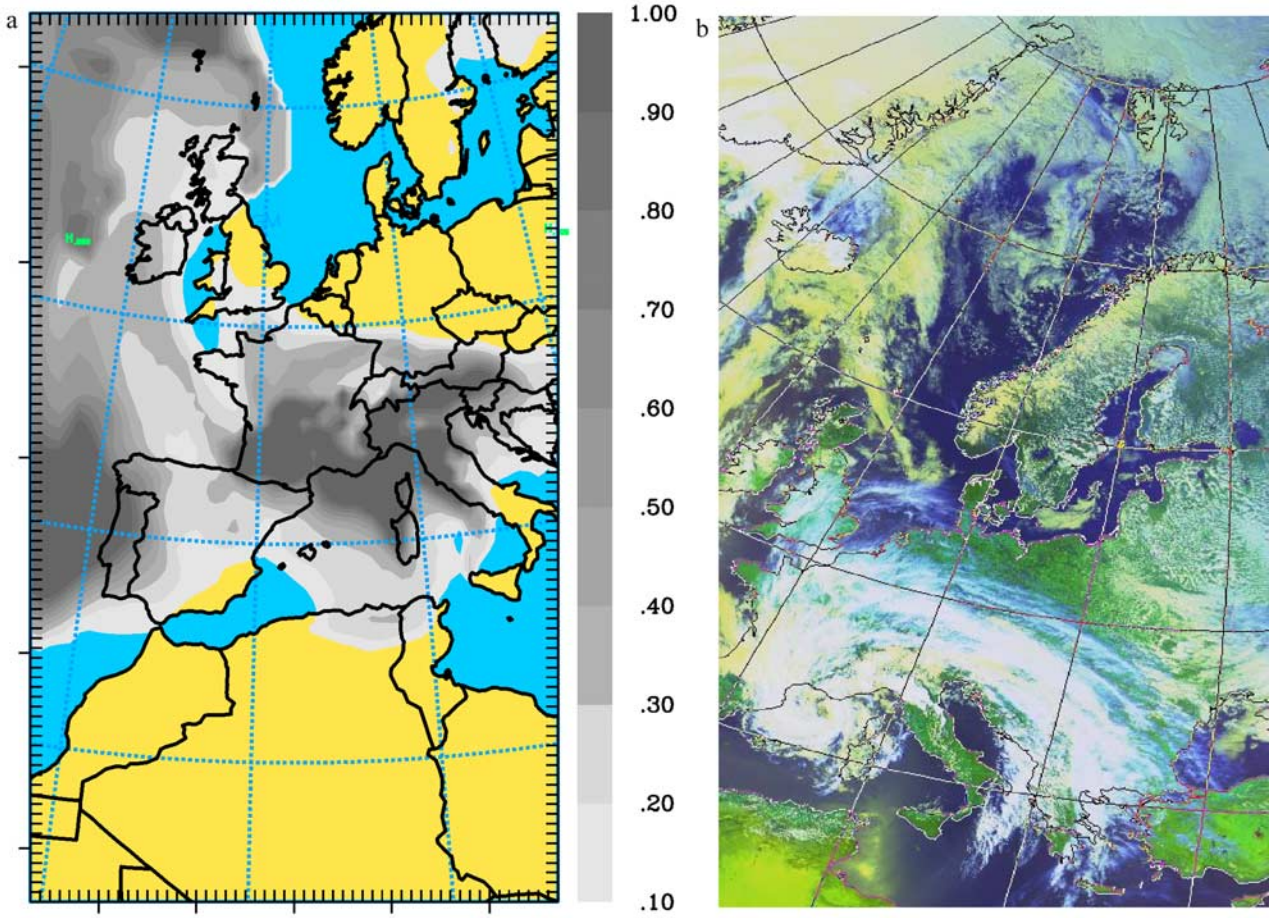

Figure 6. (a) Simulated cloud fraction in the outer model grid, for 13:48 UTC, 4 May 1999, and (b) AVHRR image in channel 7 for 13:45 UTC, 4 May 1999.

(ν) and the role of the initialization time of the simulation, sensitivity tests have been performed identical to N1, but with different values of the shape parameter (ν) and different starting time of the model runs.

5. Results From Model Simulations

[31] The simulation of the cloud pattern, performed with the aid of the RAMS model, aims at exploring the possibility of reproducing the cloud microphysical properties by utilizing conventional meteorological initial boundary conditions. As mentioned above, the discussion focuses on the results obtained for the second day of the simulation (4 May 1999) because of favorable cloud structure for model simulations. A split in the middle-level jet stream led to the formation of cirrostratus and altostratus clouds. The cloud system moved from west to east. Figure 6 illustrates a comparison of the cloud fraction in the coarser grid of the simulation, as predicted by the model on 4 May at 13:48 UTC, to the corresponding AVHRR image at 13:45 UTC.

[32] Time/height plots are employed to understand the characteristics of the cloud microphysical and dynamical processes, as well as for easy comparison between observations and model results. A vertical column in the model inner domain was extracted over a point that coincides with the position of the experimental site in Palaiseau, as indicated in Figure 5b (point C). All meteorological and cloud microphysical parameters were extracted from the model levels at time intervals of 12 min. The discussion of the results focuses on the explicitly resolved microphysical parameters and specifically on water content (LWC or IWC), number concentration (N_t) and diameters of the following categories of ice water substance: aggregates, graupel, hail, rainwater, pristine ice, snow and total ice. The patterns of particles in the liquid phase are also presented. In order to exclude any possible influence on the results of the initial conditions imposed, the time/height cross sections of all parameters are prepared for a 9-hour time period (between 6:00 and 15:00 UTC) 30 hours after the model initialization. It should be pointed out that in all figures the heights are estimated above sea level (ASL), while for the water content of all categories of ice crystals a lower limit of 0.0001 g/m^3 is assumed. Additional cross sections of air temperature, wind direction, wind speed, relative humidity and the vertical component of the wind are also provided (Figure 7).

[33] The temperature cross section shows that there was a temperature inversion from the ground up to a height of 1000m, which broke up at around 11:00 UTC (Figure 7a). The zero degree isotherm is located at about 2.8 km ASL (Figures 7a and 8). This value is comparable to the height obtained from the sounding at Trappes (Figure 9).

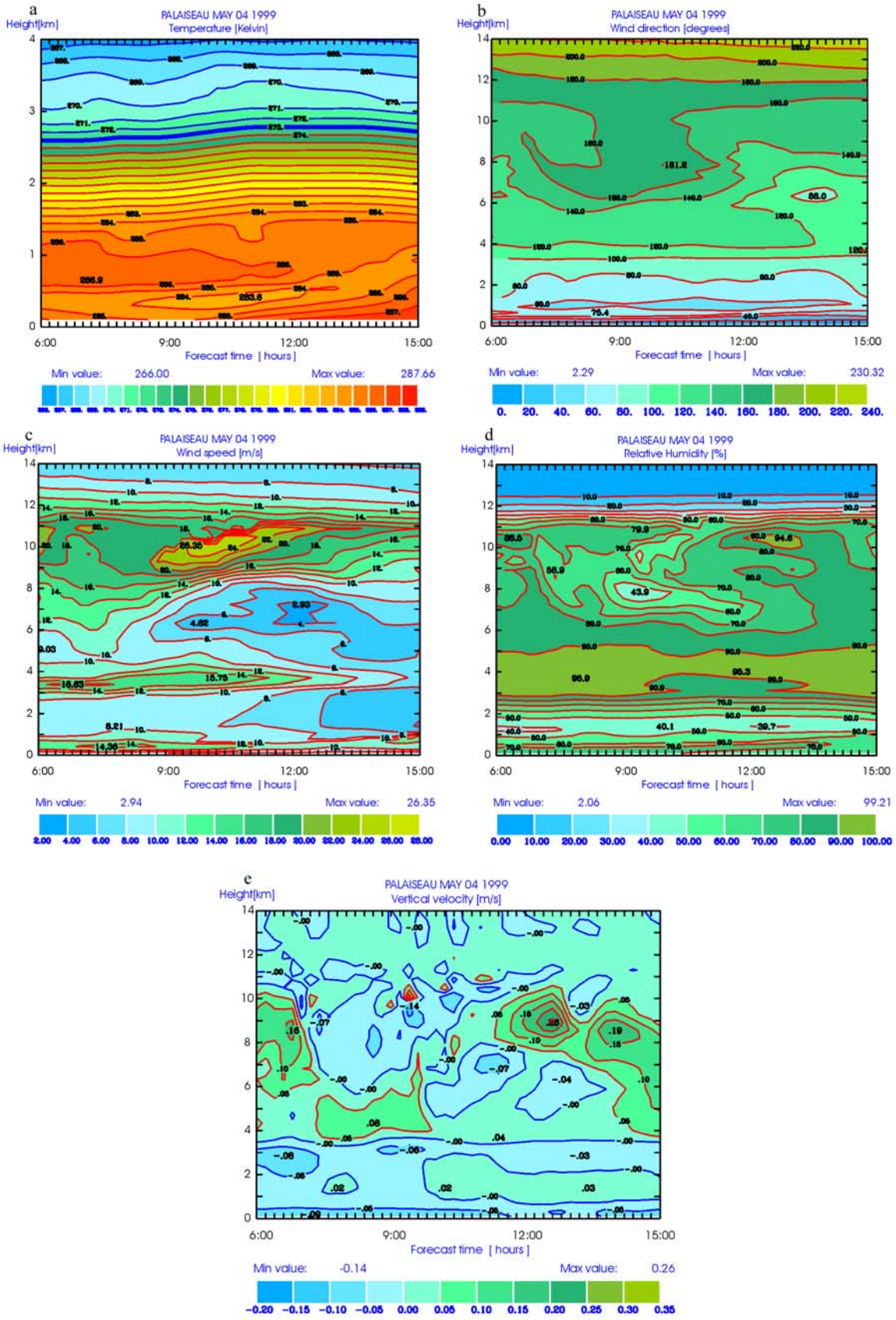

Figure 7. Time/height cross sections over the experimental site of simulated: (a) temperature (Kelvin); (b) wind direction (degrees); (c) wind speed (m/s); (d) relative humidity (%) and (e) the vertical component of wind (m/s).

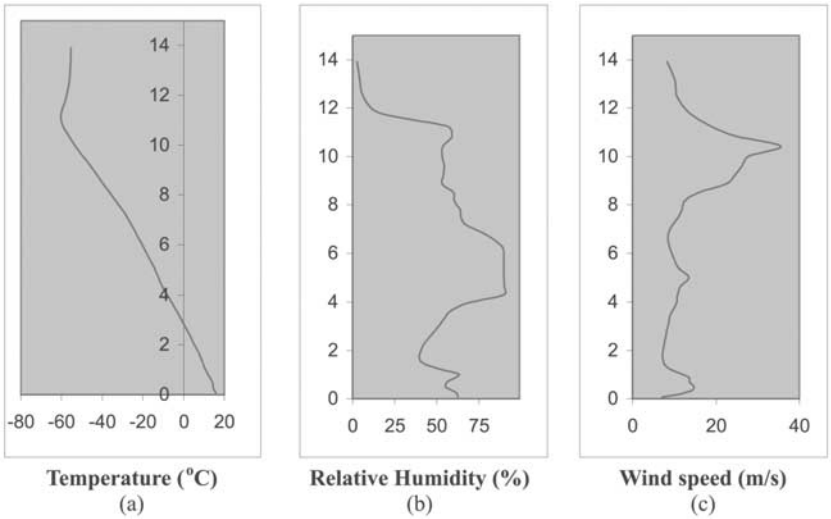

Figure 8. Vertical profiles for 00:00 UTC, 4 May 1999 of (a) temperature (°C); (b) relative humidity (%) and (c) wind speed (m/s), from model results.

[34] The wind field over the experimental site shows a strong wind shear, which might be responsible for cloud formation in the vertical during the initial stages of cloud development (Figure 7c). The maximum wind speed reaches 15.75 m/s at the cloud base (~3.5 km) and 26.35 m/s at the cloud top (~10 km), while wind direction changed with altitude from 40° up to 180° (Figure 7b).

[35] The model results show that the moisture associated with the southeasterly flow is important throughout the entire troposphere, while the largest moisture values are observed in the middle and upper troposphere. On the basis of the relative humidity (RH) values, the troposphere is divisible in three layers, namely the lower, intermediate and upper layers (Figure 7d). The lower layer extends from the ground to approximately 3 km ASL, where the cloud base is located. The air masses within this layer are, in general, quite moist with a dryer region in the middle (around 40% RH). The second layer extends from 3 to 5 km ASL. This layer is characterized by high values of RH, ranging between 90 and 95%, which indicate the existence of clouds. The third layer is between 5 and approximately 11 km, where the cloud top is located. Within this layer RH drops gradually from high values of around 90% to around 50%.

[36] The vertical component of the wind (w) is characterized by velocities ranging from −0.14 to 0.26 m/s (Figure 7e), which represent typical values for similar cloud systems.

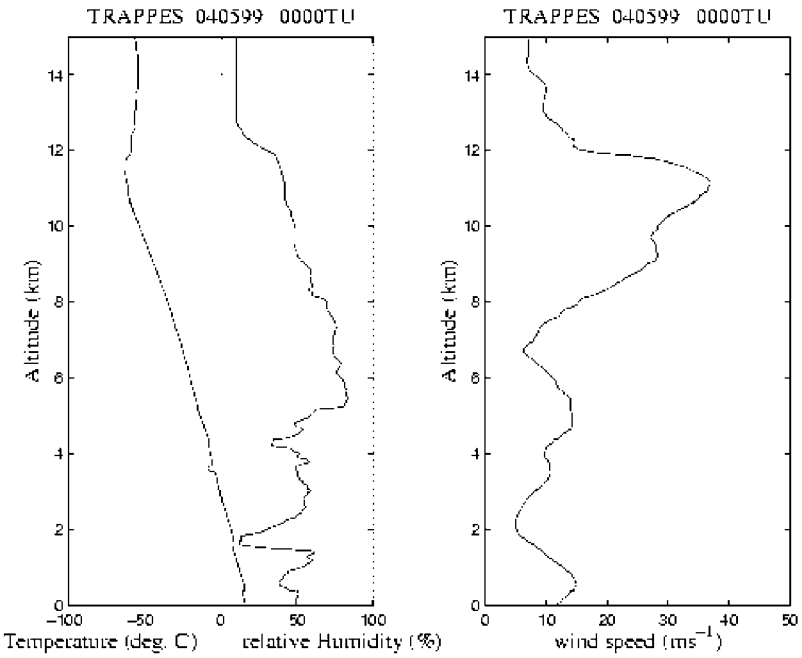

Figure 9. Vertical profiles for 00:00 UTC, 4 May 1999 of (a) temperature (°C); (b) relative humidity (%) and (c) wind speed (m/s), as obtained from the sounding at Trappes during the experimental campaign.

According to the literature [e.g., *Yuter and Houze*, 1995], the vertical velocity in stratiform regions is close to zero near the ground, while the region below the environmental 0°C is dominated by weak downdrafts. Above the vicinity of 0°C, the vertical velocity increases and crosses over zero. Weak updrafts dominate at midlevels and upper levels. According to the model results, the strongest updrafts appeared between altitudes of 6.0 and 10.0 km ASL (prior to 8:00 UTC) and in a layer between 8.0 and 10.0 km ASL (at around 12:00 UTC), consistent with the maximum ice concentrations, which will be discussed below. As stated by *McInnes and Curry* [1995], vertical air velocities less than 1 cm/s are sufficient for maintaining cloud layers. They also suggest that once the cloud is established, vertical air motion is not necessary for cloud maintenance. This indicates that clouds probably form because of upward motion within the cloud layer.

[37] In addition, vertical profiles of wind speed, temperature and relative humidity (Figure 8) have been prepared from model results over the experimental site (point C), for comparison with corresponding profiles (Figure 9) obtained from the sounding at Trappes (15 km from Palaiseau). The model reproduced the temperature field quite well, as well as the wind speed and relative humidity. However, some discrepancies were observed between the model output and the measurements for the latter two fields. More specifically, the relative humidity, as obtained from model results, is found to be approximately 10% greater than observations for the layer below 6 km ASL. Also, the modeled maximum wind speed (~35 m/s) was found at a slightly lower altitude (~10.5 km) in comparison with that obtained from the sounding (~11 km), which can likely be attributed mainly to the sparse vertical structure of the model (~1000 m vertical increment) at this altitude.

5.1. Microphysical Characteristics of the Cloud

[38] During the aforementioned time period (06:00–15:00 UTC), the atmosphere was separated into characteristic layers. The results showed that the main body of liquid water (cloud and rain) was located at low (<3 km ASL) altitudes (Figure 15), while ice particles were found further aloft (Figure 10). During the day, because of the interaction between particles in the liquid phase and ice crystals and that among crystals, aggregates appeared in an intermediate atmospheric layer (~4 km ASL). The detailed structure for each one of these categories of forms of water is discussed below.

[39] Ice crystals dominated the layer extending from 3 to 10 km ASL. The greatest amount of ice crystals were formed in zones of upward motion (see Figure 7e) and observed approximately within a layer from 6 km to 9 km before 08:00 UTC and after 10:00 UTC. This agrees well with radar observations (Figure 1a). Prior to 08:00 UTC, the IWC was as high as 0.29 g/m^3, while N_t reached a maximum of 226 #/L. The corresponding values for the time period after 10:00 UTC were 0.21 g/m^3 for IWC and 468 #/L for N_t (Figures 10a and 10b). During the period 11:00–14:00 UTC (''Merlin'' aircraft flights), the main body of ice particles was located within the layer between 6 and 10.5 km ASL. Ice particle concentration (N_t) increased with height, indicating nucleation processes at the upper cloud levels and mainly at the cloud top where the temperature was of −56°C. The cloud base was located above the freezing level, with temperatures ranging between −2 and −3°C. A three-dimensional view of the simulated cloud, which provides an extensive view of the event, is shown in Figure 11, where the top of the graph box represents the model top.

[40] Pristine ice crystals were found in the atmospheric layer between 5 km and 10.5 km ASL (Figure 12) with diameters smaller than 126 microns (Figure 12b). The maximum number concentration of small pristine ice particles (diameters smaller than 60 microns) reached 397 #/L at around 10 km ASL (see Figure 12a). At the locations where the maximum number concentrations were found, the IWC reached 0.017 g/m^3. Since pristine ice particles nucleate from vapor and grow by vapor deposition, these maxima are observed in atmospheric layers characterized by high values (~90%) of relative humidity (Figure 7d) and temperatures below −5°C. Since pristine ice number concentration (N_t) increases with height, it can be concluded that primary ice formation is likely occurring in these layers.

[41] Snow particles dominated the entire cloud body, especially the layer between 5 and 10 km ASL (Figure 13). The snow crystals form from pristine ice by vapor deposition. This is why snow was mainly observed in regions with high values of RH (Figure 7d) and below layers characterized by the largest mass and number concentration of pristine ice (Figure 12a). The modeled snow crystals exhibit a size distribution characterized by a decreasing concentration toward the large end of the size spectrum. The highest number concentration of snow crystals (135–150 #/L) appeared for a limited time (approximately 20 min) prior to 07:00 UTC (Ac cloud formation) in two levels (around 6 and 7 km), within a zone of upward motion. The snow particle diameters were less than 150 and 200 microns respectively (not shown in a figure here). The IWC in these regions was 0.14 and 0.29 g/m^3, respectively as it is shown in Figure 13. On the contrary, the large snow crystals (of diameter ~500 microns) reproduced by the model were in low concentrations (<0.8 #/L).

[42] The falling snow crystals of different sizes and corresponding fall velocities grow rapidly to form aggregates. This growth is of course associated with a reduction in the number concentration of ice particles in these layers. Aggregation produces larger ice particles, mainly within a 2 km layer above the 0°C level. Most of the aggregates were found within the lowest half of this layer (see Figures 14 and 7a), which practically diminishes between 10:00 and 13:00 UTC. Most of the aggregates have diameters ranging from 100 to 900 microns. Since the probability of adhesion of colliding ice particles increases as temperature increases to above −5°C, the maximum concentration (8.49 #/L) and IWC (0.1 g/m^3) of aggregates was observed at locations characterized by the highest values of RH (Figure 7d) and temperatures close to −5°C (4 km ASL, see Figure 7a). This is due to the fact that at these temperatures the surfaces of ice crystals become sticky and therefore the particle sizes increase sharply at temperatures above −5°C, while aggregation does not occur below −20°C [*Houze*, 1993].

[43] According to the model results, negligible quantities of graupel and hail particles appear near the cloud base with diameters less than 1400 microns. These groups of particles are treated as transitional particles between the ice and liquid phases in the RAMS microphysical model. Partial

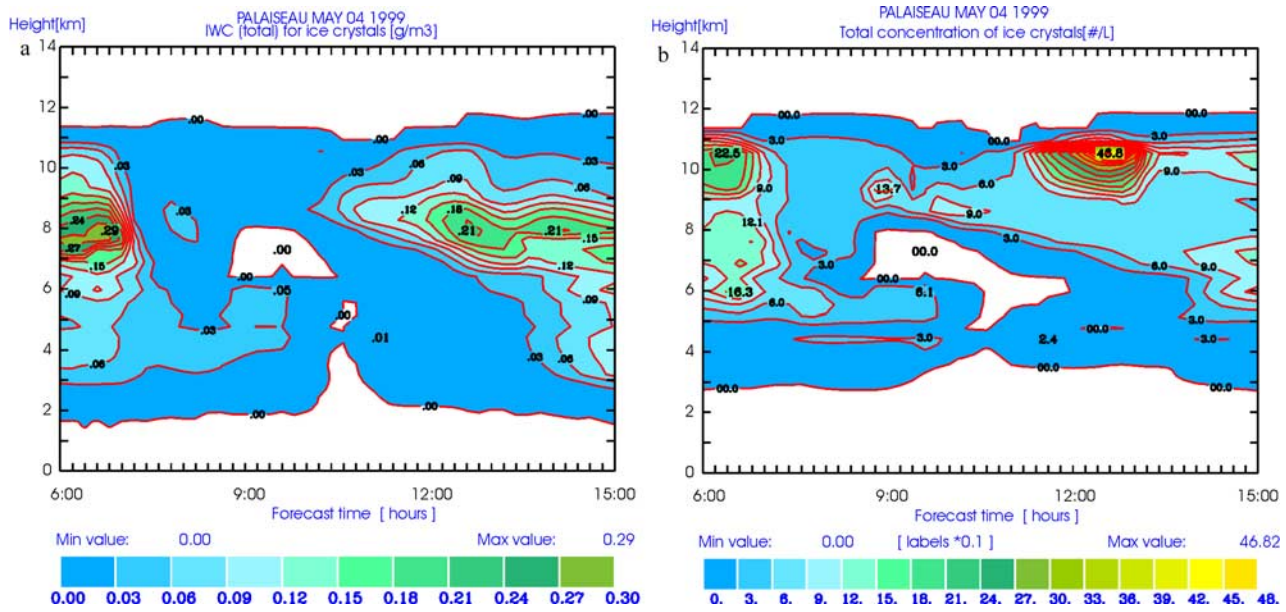

Figure 10. Time/height cross sections of (a) total ice IWC (g/m^3) and (b) concentration of total ice (#/L multiplied by 0.1), at point C in the control simulation.

melting of snow and aggregates cause some of their mass to be converted to graupel, and partial melting of graupel causes some of its mass to be converted to hail [*Walko et al.*, 1995]. They are not the results of strong updraft activity, since such a thing does not exist in this case. According to the literature [*Holroyd*, 1964; *Cotton and Anthes*, 1989; *Pruppacher and Klett*, 1997], such formations can originate at the cloud base under certain conditions, since there is some indication that aggregates of ice crystals can serve as embryos for graupel particles. Unfortunately no aircraft paths are available through this layer to verify the model results, and the available radar echoes are not considered adequate by themselves for such an interpretation.

[44] Aggregation concentrates condensate into large particles, which, upon melting, become large falling drops. The appearance of liquid water varies with height and time during the simulation period, with noticeable amounts early in the morning and in the afternoon hours (Figure 15). More specifically, N_t reached 0.155 #/L and LWC had a maximum of 0.014 g/m^3 after 14:00 UTC. Between 7:30 and 14:00 UTC, the LWC was very low, varying between 0.0001 and 0.001 g/m3. The layer of liquid water was characterized by the presence of raindrops of diameters between 600 and 900 microns. According to the literature, ice particles, upon completion of melting, collapse to raindrops of diameters typically between 1 and 2.5 mm [*Pruppacher and Klett*, 1997]. Such large raindrops cannot stay in the cloud. As shown in Figure 16, the raindrops were reaching the ground practically before 08:00 UTC and after 14:00 UTC.

5.2. Sensitivity Tests

[45] In order to gain better insight into cloud microphysics, several sensitivity tests were performed for domain selection, grid resolution and vertical structure.

[46] More vertical layers are always desirable in model simulations, especially for tests emphasizing on cloud formation processes, but the computational cost is still prohibitive. Several tests with varying numbers of vertical layers, from 30 to 65, were performed but not shown here. The vertical structure of the innermost RAMS grid was emphasized. A satisfactory vertical representation of the atmosphere with reasonable computational load was obtained with 45–50 layers.

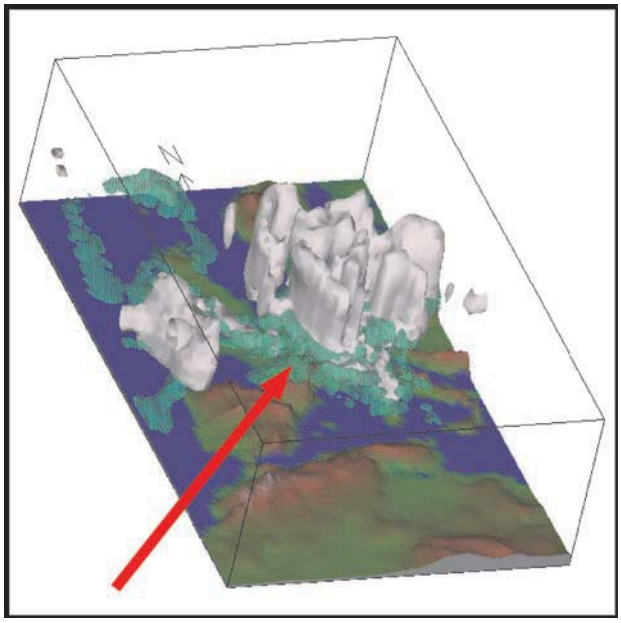

Figure 11. Three-dimensional illustration of the event for 12:00 4 May 1999, as viewed from SW. The cloud boundaries are defined by the (i) 0.03 g/kg iso-surface of total IWC (in gray color) and (ii) 0.03 g/kg iso-surface of total LWC (in green color). The red arrow indicates the location of the experimental site.

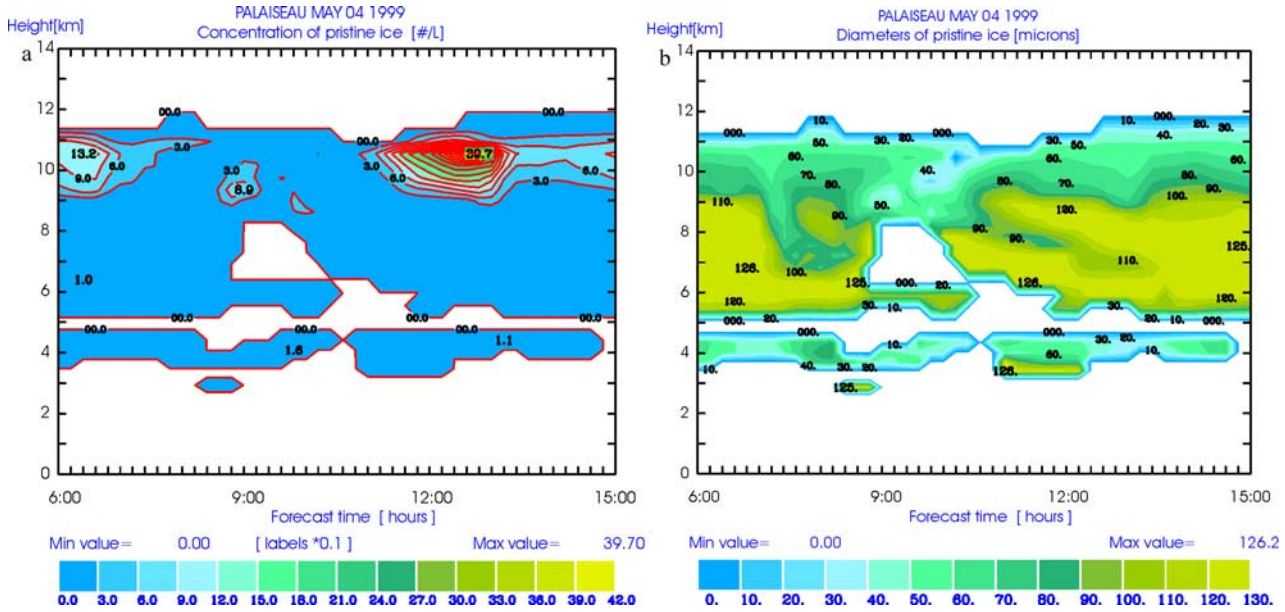

Figure 12. Time/height cross sections of (a) concentration of pristine ice (#/L multiplied by 0.1) and (b) pristine ice diameters (microns), at point C in the control simulation N1.

[47] The atmospheric model solution may be relaxed toward the analyzed data during time integration. The strength of the nudging is defined as (I-M)/T, where I is an initialization file data value at a particular location, M is the corresponding model value, and T is a user specified relaxation timescale. Several tests were performed with nudging periods of 3, 6, 12 and 24 hours. The best model results corresponded to the largest nudging period (24 hours). This led to the conclusion that some mesoscale structures are important in the cloud structures observed. The use of the nudging option with a small nudging period enhances the role of synoptic-scale features and eliminates local structures. Hence a 24-hour nudging period, which is practically negligible, was used for the model simulations.

[48] In a second stage, sensitivity tests were also performed in order to investigate the influence of the shape parameter ν on the microphysical structure of the cloud. Larger values of the shape parameter affect the microphysical characteristics of the precipitation process [*Krichak and Levin*, 2000]. Sensitivity studies were also performed in relation to the initialization of the simulation. In this paper only the results of the most important additional runs will be discussed. The differences in the model setup of the additional runs are summarized in Table 3.

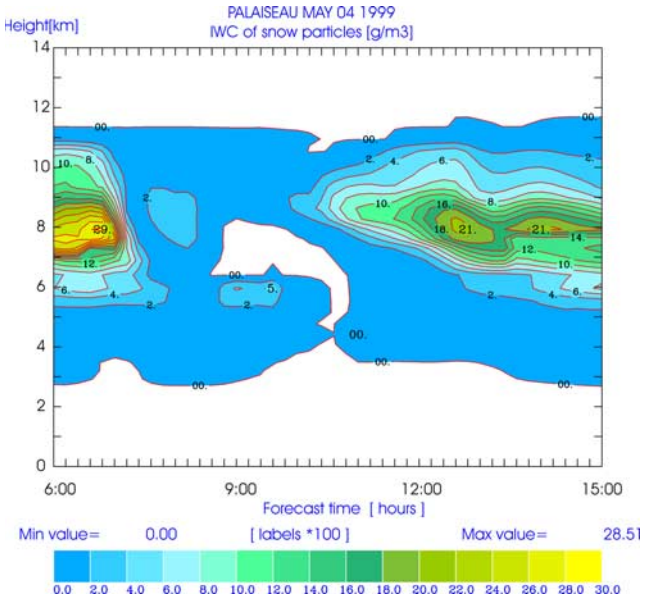

Figure 13. Time/height cross section of IWC of snow (g/m^3 multiplied by 100), at point C in the control simulation N1.

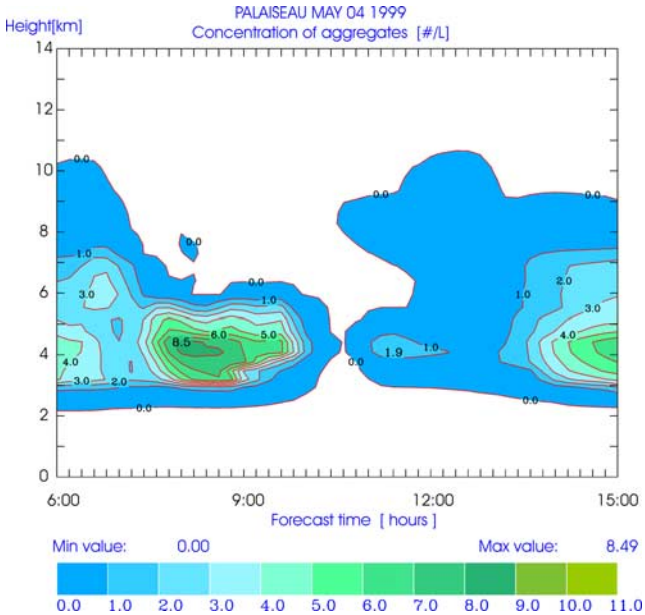

Figure 14. Time/height cross section of concentration of aggregates (in #/L), at point C in the control simulation N1.

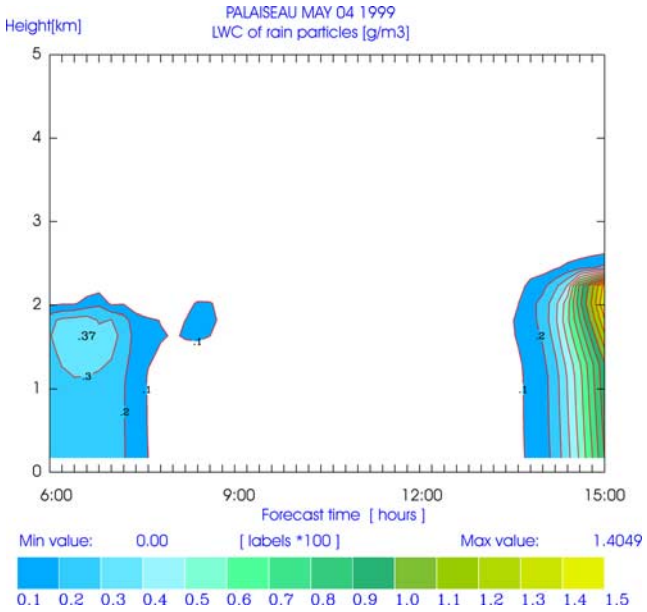

Figure 15. Time/height cross sections of LWC of rain-droplets (g/m^3 multiplied by 100), at point C in the control simulation N1. A lower limit of 0.001 g/m^3 is assumed.

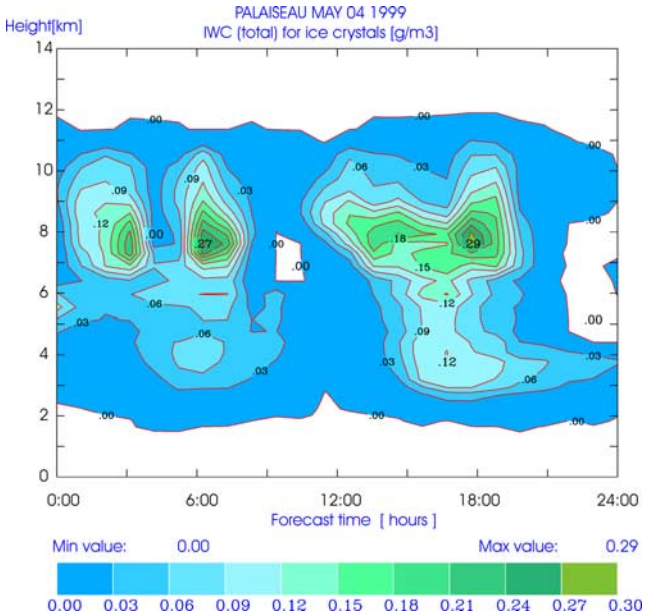

Figure 17. Time/height cross section of total ice water content (g/m^3), at point C in control simulation N1 with $\nu = 1$.

[49] All meteorological and cloud microphysical parameters were extracted from the model levels at time intervals of one (1) hour. The discussion of the results focuses on ice water content and the number concentration of total ice particles. These results are presented in the form of time/height cross sections (Figure 17). The control run (hereafter referred as run N1) corresponds to the previously described simulation in which the ν-shape values for all hydrometeors were equal to 1.

5.2.1. Simulation ST1

[50] Time/height cross sections have been prepared for 24 hours, in a similar fashion to those prepared for the control run N1. Despite the fact that there are similarities between the two runs (N1 and ST1) in terms of cloud geometry, there are differences in the local maxima of total ice water content in both time and space (see Figures 17 and 18). In general, the ST1 simulation produces larger values of IWC and number concentration than N1 at the lower levels of the cloud deck. A time shift is also noticeable for the appearance of the afternoon maxima. At the higher layers (>8 km) of the atmosphere the ν-shape value does not appear to affect the distribution of small particles (especially of the smaller pristine ice). On the contrary, the microphysical characteristics of the larger hydrometeors are found to be sensitive to the variations of the parameter (ν) of the particle spectra. During this run (ST1, $\nu = 3$) high values of the number concentration and mixing ratios (Figure 18) are found in the layer between 4 and 6.5 km, which are not observed in the run N1 ($\nu = 1$).

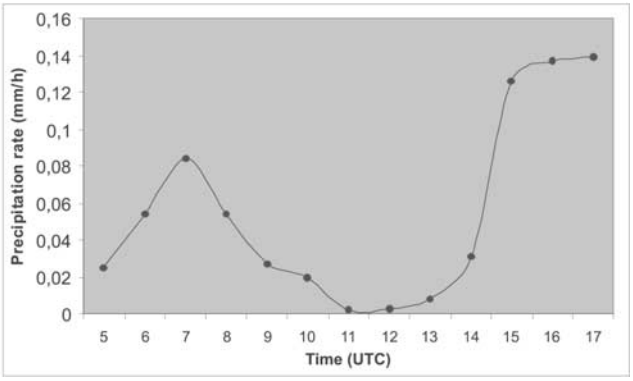

Figure 16. Precipitation rate over the experimental site for 4 May 1999 (mm/hr), as resulted from control simulation N1.

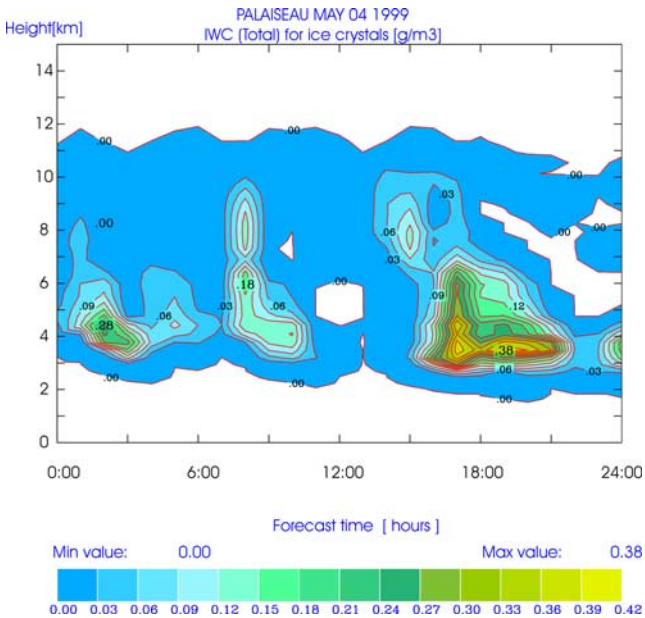

Figure 18. Time/height cross section of total ice water content (g/m^3), at point C in the ST1 simulation with $\nu = 3$.

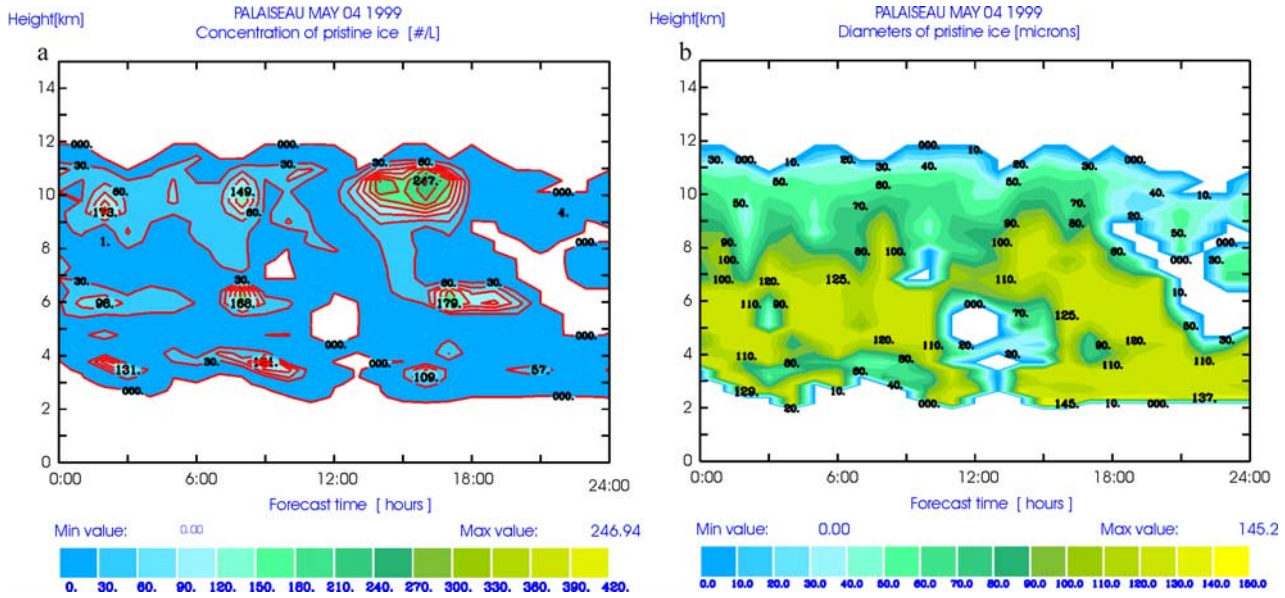

Figure 19. Time/height cross sections of (a) concentration of pristine ice (#/L) and (b) diameter of pristine ice (microns), at point C in ST1 simulation with $\nu = 3$.

[51] Variations of the ν-shape parameter did not affect also the distribution of the smaller pristine ice particles. On the contrary, the microphysical characteristics of the larger pristine ice particles appear to be sensitive to these variations. In the case of ST1, high concentrations of large pristine ice particles are produced at the lower and middle levels of the cloud deck, which are not reproduced by the N1 simulation (Figures 19a and 19b). The growth of pristine ice leads to the production of an increased load of snow particles near the bottom of the cloud deck. However, these particles did not have the time to grow enough because of the strong aggregation that was observed at these altitudes as it is shown in Figure 20.

[52] Summarizing the most important differences between two runs (ST1 and N1) were: a) a time shift occurred in the appearance on the afternoon maxima and b) considerably higher values of number concentration and IWC at the lower and middle levels of the cloud deck were observed for run ST1. With this microphysical configuration, the larger and heavier particles are favored at the lower levels of the troposphere.

5.2.2. Simulation ST2

[53] In general, the simulation ST2 reproduced the basic cloud formation (e.g., cloud boundaries) with differences within reasonable limits (in comparison to N1). The most important differences concern the local maxima of IWC, mainly at the lower levels of the atmosphere where, in general, slight higher values are observed for run ST2 (see Figures 21a and 17). High values of number concentration have also been produced during the first 9 hours of the ST2 run as shown in Figure 21b. This is due to the initial concentration of activated cloud droplets used at the initialization stage of the simulation, which is 24 hours later than run N1. The condensates at these locations were mainly composed of small ice crystals (principally pristine ice), which were formed by the freezing of activated initially cloud droplets. In general, the larger differences occur during the first 3 to 6 hours of the simulation.

[54] It appears that cloud formation at the local scale is influenced by the large-scale initial conditions used in the model simulation (different analysis fields).

Table 3. Differences in the Model Setup for the Additional Simulations

Name of the Run	Value of the Shape Parameter ν	Initialization Time
N1	1	00:00 UTC (3 May 1999)
ST1	3	00:00 UTC (3 May 1999)
ST2	1	00:00 UTC (4 May 1999)
ST3	2	00:00 UTC (4 May 1999)

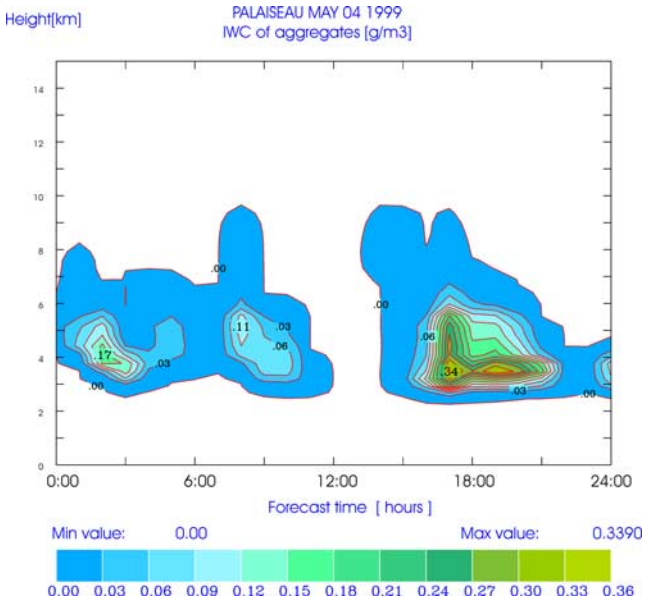

Figure 20. Time/height cross sections of IWC of aggregates (g/m^3), at point C in ST1 simulation with $\nu = 3$.

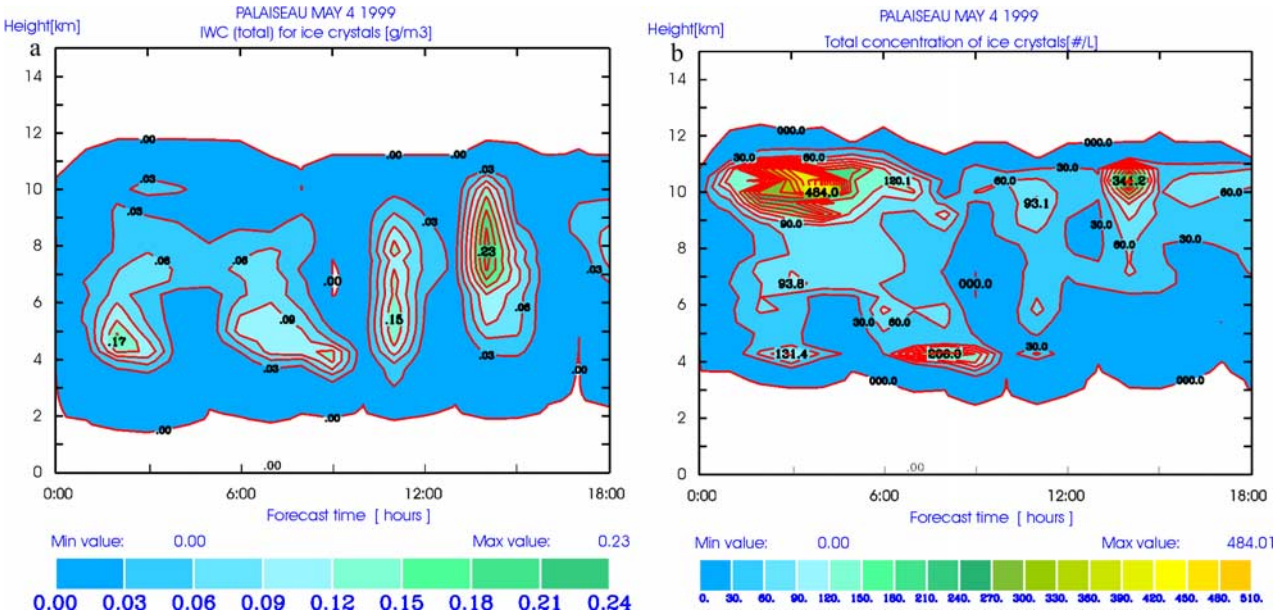

Figure 21. Time/height cross sections of (a) total ice water content (g/m^3) and (b) number concentration (#/L), at point C in the ST2 simulation with $\nu = 1$ (the run starts 24 hours later than the control run N1).

5.2.3. Simulation ST3

[55] As in run ST2, the initialization time of the model for run ST3 was 4 May, 00:00 UTC. The only difference in the model setup between the two simulations was that for the ST3 run the ν-shape parameter was equal to 2. In general, substantial differences exist between these two runs (ST2 and ST3), namely in the vertical structure as well as in the timing of the maximum IWC values, mainly after the first 9 hours of the simulation (see Figures 21a and 22). Prior to 09:00 UTC there are similarities between the two runs. The most pronounced differences appear in the amount of the total ice water content, with slightly higher values in the middle troposphere and lower values in the upper troposphere for run ST3 (Figures 21a and 22). There is also substantial deviation from the N1 simulation after 09:00 UTC (Figure 17) for the same reasons. These results support the idea that cloud formation is influenced by the value of the ν-shape parameter on timescales of just a few hours.

[56] In conclusion, the sensitivity tests showed that the microphysical structure of the cloud is affected by the selection of the shape parameter ν, as well as by the initialization time of the simulation.

5.3. Comparison With Remote Sensing Data

[57] The spatial and temporal variability of the phenomena produced by the N1 simulation (control run) fit better with the available observational data (radar reflectivity), especially the vertical distribution of IWC and ice particle concentration within the lower layer of the cloud formation. This is due to the fact that the cloud composition in this specific case is dominated by pristine ice and snow. According to the Marshal-Palmer family of curves, $\nu = 1$ is appropriate for obtaining maximum number concentrations in the vicinity of smaller diameter cloud particles. More specifically, in the radar section (Figures 1a and 1b) is shown that precipitating ice particles produce "fallstreaks" by 08:00 UTC at a height near the 0°C level (at about 2800 m). The phenomenon of "fallstreaks" is common in altocumulus cloud formations during the later stages of their lifetimes [*Houze*, 1993]. A sudden increase of the particle fall velocities below this height indicates a change of the particle composition from ice crystals to water droplets. As discussed by *Pelon et al.* [2001], around this height the LDR drops toward the value of cross polarization isolation. Because of the limited rate at which released latent heat can be dissipated to the surrounding air, the ice crystals must

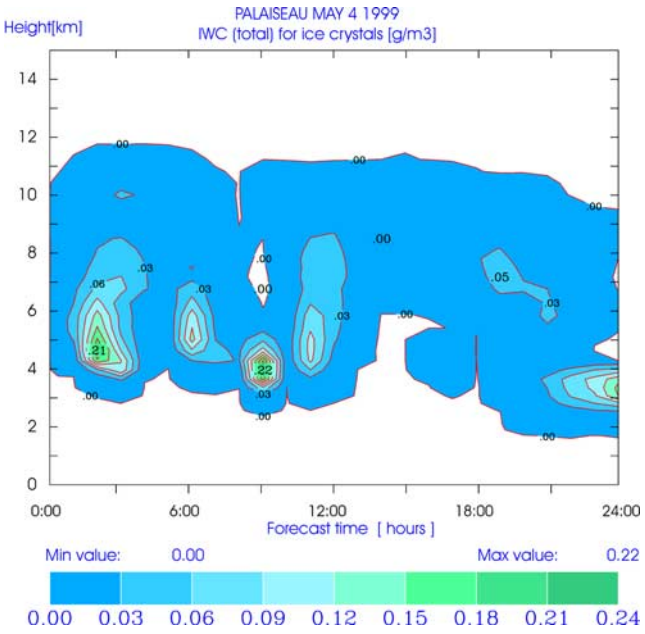

Figure 22. Time/height cross section of total ice water content (g/m^3), at point C in simulation ST3 with $\nu = 2$ (the run starts 24 hours later than the control run N1).

Table 4. Leg-Averaged Values and Standard Deviations of Temperature, Wind Speed, and Wind Direction and Averaged Values ("Data" Columns) and Standard Deviations of the Model Results at Altitudes Close to the Leg Altitude ("Model" Columns)

	Temperature, °C/Standard Deviation		Wind Speed, m/s/Standard Deviation		Wind Direction, deg/Standard Deviation	
Leg [Z(km)]	Data	Model	Data	Model	Data	Model
1 (6.0)	−18.68/0.05	−18.94/0.11	6.03/0.38	5.43/0.27	131.12/4.16	128.71/2.96
2 (6.4)	−20.97/0.09	−20.71/0.18	5.69/0.43	4.41/0.16	150.34/7.24	134.69/4.14
3 (7.0)	−25.45/0.05	−25.79/0.05	7.54/0.60	4.71/0.29	143.48/4.58	131.05/1.85
4 (7.6)	−30.37/0.04	−30.93/0.05	8.35/0.66	6.90/0.08	150.80/3.34	138.64/0.75
5 (7.9)	−32.98/0.12	−33.51/0.03	7.78/0.43	8.55/0.67	162.76/3.68	138.35/1.26
6 (8.2)	−35.57/0.04	−34.73/0.04	8.18/0.51	9.32/0.3	165.22/1.55	145.49/1.88

fall several hundred meters in order to completely melt. This distance is typically around the +5°C level [*Pruppacher and Klett*, 1997]. From the model results, liquid water starts to appear at around 2 km ASL that corresponds to the +5°C level (Figures 7a and 15).

[58] The lidar vertical profiles can also be used for verification of the model results. As it was discussed in section 2 the highest backscatter is evident between 3 and 3.5 km ASL (see Figure 2). This intense backscatter is approximately 1 km higher than the layer where small amounts of liquid water were found in the model simulation (Figure 15) and close to the bottom of the layer where the aggregates begin to melt (see Figure 14). On the basis of this combination of model results and lidar echoes (assuming that small amounts of liquid water cannot block the lidar pulse into the melting layer), it can be concluded that the maximum lidar backscatter is coming from the area where the melting of aggregates begins.

5.4. Comparison With Aircraft Data

[59] In order to further investigate the model results in both space and time, they are compared to airborne measurements of: temperature, wind speed, wind direction, ice water content (IWC) and particle number concentrations. The data were collected during six constant-altitude flight legs (see Table 4) by the "Merlin" aircraft from Meteo-France, which was equipped with a GKSS cloud particle measuring system with three sizing probes, as described in Table 2. The aircraft collected data over an area around the experimental site with a true air speed on the East-West axis of about 50 m/s. The model data was extracted at model levels close to the altitudes of the flight legs and averaged over four grid points within the area covered by the aircraft flight.

[60] Initially, leg-averaged measurements (approximately 300-s time intervals) were compared with model results for three meteorological fields: temperature, wind speed and direction. The averaged model values were found to be comparable with the leg-averaged measurements. The temperature field, as produced by the model, was found to agree fairly well with the aircraft measurements (see Table 4). The wind speed also compared well enough with the measurements. More specifically, the modeled values of wind speed were slightly smaller than the observations at lower altitudes and slightly greater at upper levels, with the exception of the third flight-leg. For this flight-leg the model reproduced the wind speed significantly lower (37%) than the aircraft measurements. Wind direction differences are within a range of less than twenty degrees throughout the entire layer where measurements were taken.

[61] In a second phase, the data was analyzed over 50-s averaging intervals for every flight leg over specific grid points within the model inner domain, coinciding with the area covered by the "Merlin" flights. This corresponds to scale length of 2.5 km, which coincides with the horizontal grid increment in the inner model grid. The results are comparable to those of the initial comparison presented above (Figure 23).

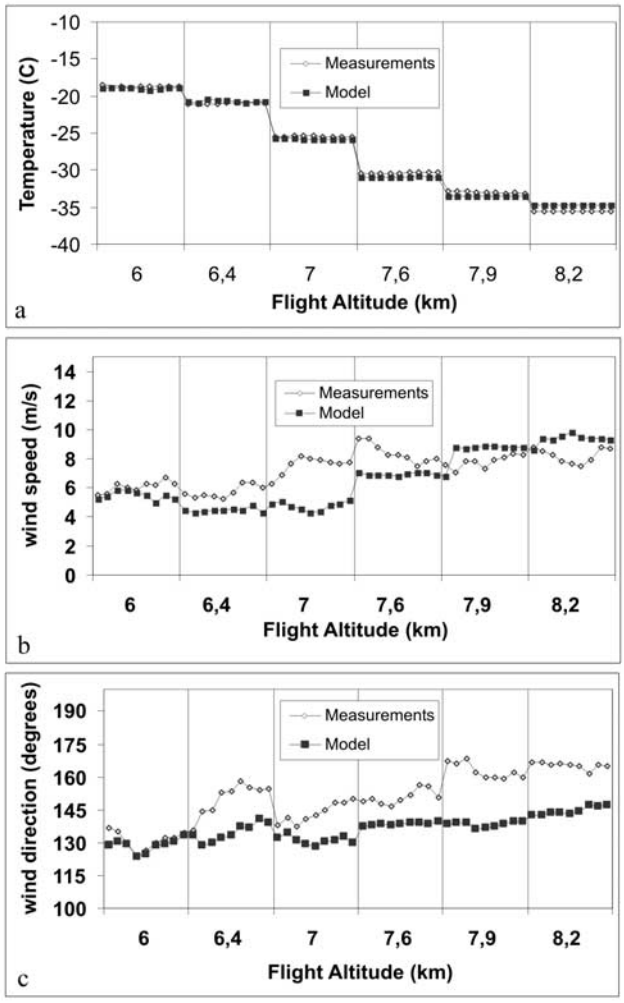

Figure 23. Comparison between aircraft measurements (averaged values on 50-s intervals) and model results of (a) temperature, (b) wind speed and (c) wind direction. The numbers on the *x* axis indicate the constant altitude of the flight legs.

Table 5. Size Range of Ice Crystals, as Grouped for Comparisons

Particle Grouping	Size Range
first size bin	2–47 microns
second size bin	25–800 microns
third size bin	200–6400 microns

[62] For better comparison of the microphysical model results to the observations, the modeled ice particles were grouped into three bins according to their diameter (Table 5), corresponding to the size range of the measuring system (Table 2). There is some overlap between the three bins of the GKSS probes, which makes the division of the modeled particles very difficult. However, a comparison can be made and useful conclusions can be drawn.

5.4.1. Small-Size Particles (2 < D < 47 Microns)

[63] The shape and concentration of the small-size ice particles play an important role in the earth's climate [*Cooper*, 1991]. Unfortunately, there are many uncertainties in measuring particle characteristics related to the current measuring systems. Because of this, *Kinne et al.* [1992] suggested that new aircraft instrumentation must be developed for the detection of ice crystals with diameters ranging from 5 to 50 microns. A recent discussion about the properties of small-size particles is also given by *Gultepe et al.* [2001].

[64] For the present work the characteristics of small-size ice particles were measured by an FSSP-100 probe (see Table 2). The FSSP is designed to measure droplet characteristics although it responds significantly to ice particles. Details and uncertainties related to the FSSP measurements are given by *Baumgardner et al.* [1985]. As discussed by *Gardiner and Hallett* [1985], false counts due to ice particles could be as high as two or three orders of magnitude greater than the actual ice crystal number concentration. In this work the comparison of the small-size particles shows that the modeled IWC and number concentration deviate significantly from the measurements, with the model values being much smaller. This deviation can be attributed either to the reduced accuracy of the measuring system or to the model parameterization or both of them. Since the uncertainties in the small-size particle measurements are quite high, the comparison with model values is considered as meaningless.

5.4.2. Medium-Size Particles (25 < D < 800 Microns)

[65] Modeled IWC and number concentration of ice crystals were averaged over 50-s intervals and compared to modeled IWC and number concentration. The modeled IWC and number concentration were found to be comparable with the measured values (Figure 24). The simulated IWC values compare quite well with those derived from measurements for all the flight-legs. The modeled values range from 0.02 to 0.177 g/m^3, while the measurements range from 0.03 to 0.192 g/m^3 (Figure 24a). Similar results are obtained when comparing number concentration during the first, second, third, and sixth flight-legs. Model values, extracted at altitudes corresponding to those of the flight-legs, range from 19.5 to 75 #/L, while the measured values range from 24.5 to 117 #/L (Figure 24b). For the remaining two flight-legs, the model significantly underestimated (by approximately 46%) the number concentration. This may be due to the fact that at these altitudes the model reproduced larger particles than the measurements of the OAP-2D2-C probe. The majority of the ice crystals in the middle and upper atmospheric levels were snow particles with diameters ranging between 200 and 350 microns, while the measured diameters were found to vary within the interval 80 to 200 microns [*Pelon et al.*, 2001].

5.4.3. Large-Size Particles (200 < D < 6400 Microns)

[66] A similar comparison was made as for the large-size particles (Figure 25). The simulated IWC and number concentration compare quite well with the observations for the four flight-legs at lower altitudes. The modeled values are found to range from 0.021 to 0.054 g/m^3, while the measurements range from 0.029 to 0.09 g/m^3 (Figure 25a). The differences are also comparably small for the number concentration of ice crystals. The modeled values range between 0.75 and 4.15 #/L. For the same altitudes, the measurements range between 1.32 and 4.25 #/L (Figure 25b). However, during the two flight legs at higher altitudes, the model results deviate significantly from the observations. These differences may be attributed to the limited capability of the numerical model near the cloud boundaries or possibly to the disturbances caused by the aircraft path (ascending). It has been asserted that the passage of an aircraft through a cloud might result in the production of ice crystals [e.g., *Rangno and Hobbs*, 1983; *Woodley et al.*, 1991; *Kelly and Vali*, 1991; *Sassen*, 1991; *Foster and Hallett*, 1993]. It was demonstrated that the ice could be formed by the homogeneous freezing of cloud droplets due to the strong adiabatic expansion and cooling near the propeller tips. Ice crystals are also formed by a secondary mechanism through heterogeneous nucleation when cooling in the

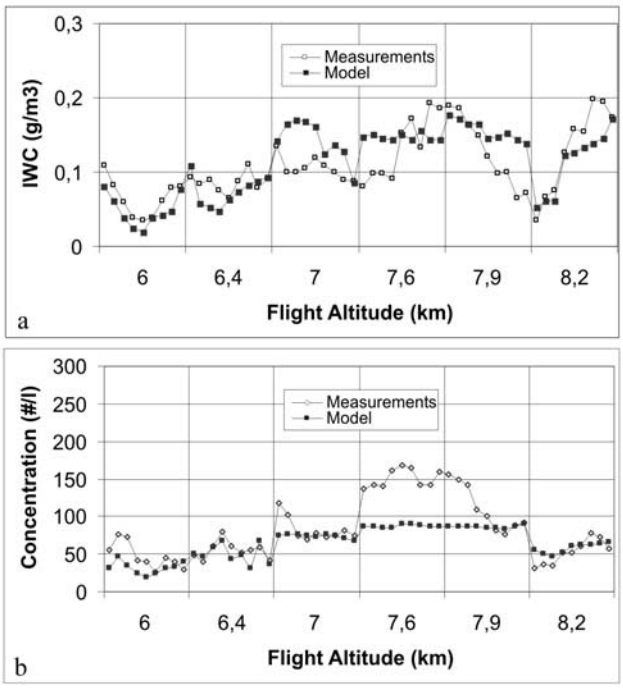

Figure 24. Comparison between aircraft measurements (averaged values on 50-s intervals) and model results of (a) IWC and (b) number concentration of medium-size particles. The numbers on the *x* axis indicate the constant altitude of the flight legs.

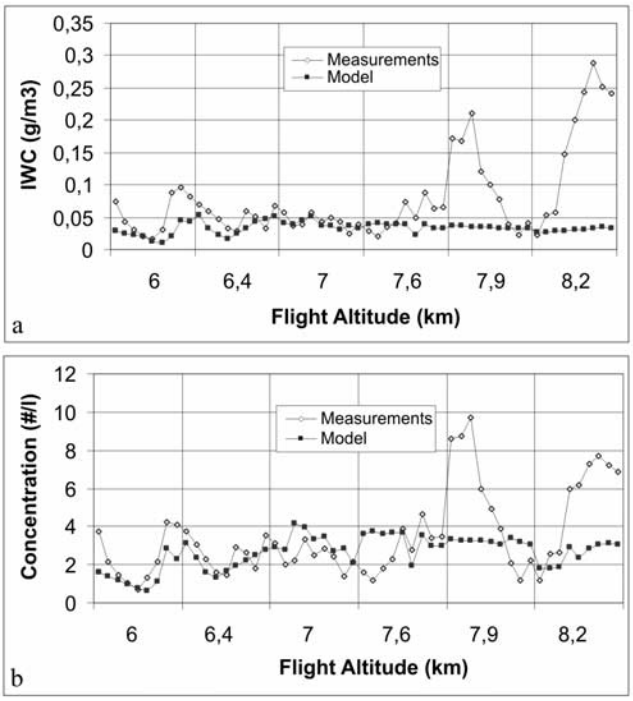

Figure 25. Comparison between aircraft measurements (averaged values on 50-s intervals) and model results of (a) IWC and (b) number concentration of large-size particles. The numbers on the *x* axis indicate the constant altitude of the flight legs.

propeller tip vortex is not strong enough to stimulate homogeneous nucleation. The passage of the aircraft in combination with small updrafts observed at these locations (Figure 7e) could produce a number of large particles at the upper atmospheric levels.

6. Summary and Conclusions

[67] In this paper an attempt was made to recover various microphysical cloud properties with the aid of a state-of-the-art atmospheric model and conventional atmospheric observations. More specifically, the RAMS modeling system was used in hindcasting mode. An independent data set was used for model validation. This data set is based on radar and lidar observations, as well as on airborne data.

[68] On 4 May 1999, the GKSS 95 GHz cloud radar observed a homogeneous cloud structure within the layer 3.5–10 Km for the time period 06:00 to 15:00 UTC. A strong wind shear over the experimental site may have been responsible for cloud formation in the vertical during the initial stages of the cloud development. The model simulation showed that the lower levels of the cloud deck (the layer between 3–5 Km) were characterized by a concentration of aggregates, while snow particles dominated at levels above the height of 5 Km. Pristine ice particles of small diameter and low density prevailed throughout the cloud body with the highest concentrations at the cloud top (~10 Km). The strongest updrafts occurred at altitudes and time periods where the maximum ice concentration was observed. This indicates that additional cloud formations occur because of upward motions within the cloud layer.

[69] In comparison to the available observational data (radar reflectivity), the model simulates well the spatial and temporal variability of the cloud parameters, especially the vertical distribution of IWC and ice crystal concentration within the lower cloud layers. Comparisons with data collected at the middle and upper cloud levels showed that the detailed cloud features observed are well reproduced by the model.

[70] The modeled temperature field compared fairly well to the measurements, while the wind speeds were slightly smaller than the observations at the lower altitudes with the exception of the third flight leg, where more serious differences were observed. At the upper cloud levels, the modeled wind speeds were slightly greater. Although, the differences in wind direction were not significant.

[71] The simulated IWC values for medium-size particles compare well enough to those derived from measurements, for all the flight-legs. Similar results were obtained for number concentration, but some discrepancies were observed at altitudes near the cloud top where the model significantly underestimated (~46%) the number concentration. This is likely due to the fact that at these altitudes the model reproduced larger particles than what the OAP-2D2-C probe measured.

[72] For large-size particles, the differences between the simulated and measured IWC and number concentration are comparably small for the flight-legs at lower altitudes. During the flight-legs at higher altitudes, the model results deviate substantially from the observations. These differences between may possibly be attributed to the limited capability of the model near the cloud boundaries or to disturbances caused by the upward aircraft flight.

[73] Finally, comparison of the small-size particles shows that the modeled IWC and number concentration deviate significantly from the measurements, with the model values being much smaller. This deviation can be attributed to the reduced accuracy of the measuring system or to the model parameterization or both.

[74] Sensitivity tests showed that cloud formation at the local scale is affected by the time of model initialization during the initial stages of the simulation (a few hours). The microphysical structure of the cloud is also influenced by the selection of the -shape parameter. The best fit with observational data, especially at the lower cloud levels, was obtained with the shape parameter (ν) equal to 1, which favors the development of particles with small diameters. This is particularly appropriate for the cloud composition of this specific case, which consisted mainly of pristine ice and snow particles. Minor changes in the data sets related to the model dynamics did not substantially influence the microphysical characteristics of the cloud formation. However, model domain characteristics like domain size and grid granulation are important under certain circumstances.

[75] In conclusion, the activation of the full microphysics package of RAMS resulted in a relatively accurate reproduction of the cloud band within the layer seen by the radar. The present status of advanced modeling systems, like the one used in the present study, is considered as satisfactory for day to day usage on describing cloud formations. Certainly, a more extensive evaluation is necessary (e.g.,

validation for larger time periods with more data from different cloud formations).

[76] **Acknowledgments.** This work was partially supported by the EU funded project CARL (EU/DGXII-contract ENV4-CT95-0036). The data collected during the experimental campaign is a joint effort of the other partners involved in this project (IPSL, GKSS, KNMI). The researchers of these groups are acknowledged for this work. More specifically, we would like to thank J. Pelon and M. Quante for the exellent cooperation we had so far and for the preparation of the graphical representation of the radar and lidar data. Partial support was also from projects ADIOS (EU/DGXII-contract EVK3-CT2000-00035) and MAMCS (EU/DGXII-ENV4-CT97-0593). This work is considered as a necessary validation procedure of the RAMS microphysical package because it is used in applications, such as in-cloud chemistry and deposition of various species ranging from conventional pollutants (e.g., deposition of particulate matter as studied within the framework of the ADIOS project http://forecast.uoa.gr/activeprj.html) to heavy metals (e.g., mercury within the framework of the MAMCS project http://forecast.uoa.gr/activeprj.html). One of the authors (E. Mavromatidis) wants to thank the Hellenic Ministry of Education and Religion for providing him the absence of leave in order to complete this study. We would like to thank C. J. Tremback and R. L. Walko for their continuous support on various issues related to RAMS. Thanks are also given to M. O'Connor for his assistance to improve the quality of this manuscript. Finally, we would like to thank the anonymous reviewers for their useful and constructive suggestions.

References

Baumgardner, D., J. W. Strapp, and J. E. Dye, Evaluation of the forward scattering spectrometer probe. II: Corrections for coincidence and dead-time losses, *J. Atmos. Oceanic Technol.*, *2*, 626–632, 1985.

Chen, C., and W. R. Cotton, A one-dimensional simulation of the stratocumulus-capped mixed layer, *Boundary Layer Meteorol.*, *25*, 289–321, 1983.

Clark, T. L., and R. D. Farley, Severe downslope windstorm calculations in two and three spatial dimensions using anelastic interactive grid nesting: A possible mechanism for gustiness, *J. Atmos. Sci.*, *41*, 329–350, 1984.

Cooper, W. A., Research in cloud and precipitation physics: Review of the U.S. theoretical and observational studies, 1987–1990, *Rev. Geophys.*, *29*, supplement, 69–79, 1991.

Cotton, W. R., and R. A. Anthes, *Storm and Cloud Dynamics*, Academic, San Diego, Calif., 1989.

Flatau, P. J., G. J. Tripoli, J. Verlinde, and W. R. Cotton, The CSU-RAMS Cloud Microphysical Module: General theory and code documentation, *Atmos. Sci. Pap. 451*, 88 pp., Dep. Atmos. Sci., Colo. State Univ., Fort Collins, 1989.

Foster, T. C., and J. Hallett, Ice crystals produced by expansion: Experiments and application to aircraft-produced ice, *J. Appl. Meteorol.*, *32*, 716–728, 1993.

Fowler, L. D., and D. A. Randall, Liquid and ice cloud microphysics in the CSU general circulation model: 2. Impact on cloudiness, the Earth's radiation budget, and the general circulation of the atmosphere, *J. Clim.*, *9*, 530–560, 1996a.

Fowler, L. D., and D. A. Randall, Liquid and ice cloud microphysics in the CSU general circulation model: 3. Sensitivity to model assumptions, *J. Clim.*, *9*, 561–586, 1996b.

Fu, Q., and K. N. Liou, Parameterization of the radiative properties of cirrus clouds, *J. Atmos. Sci.*, *50*, 2008–2025, 1993.

Fujiyoshi, Y., M. Quante, O. Danne, and E. Raschke, Some properties of deep stratiform ice cloud revealed by 95 GHz GKSS cloud radar: A case study, *Contrib. Atmos. Phys.*, *72*(1), 113–125, 1999.

Gardiner, B. A., and J. Hallett, Degradation of in-cloud forward scattering spectrometer probe measurements in the presence of ice particles, *J. Atmos. Oceanic Technol.*, *2*, 171–180, 1985.

Gultepe, I., and A. Heymsfield, Vertical velocities within a cirrus cloud from Doppler lidar and aircraft measurements during FIRE: Implications for particle growth, paper presented at Tenth International Cloud Physics Conference, Dtsch. Wetterdienst, Bad Homburg, Germany, 1988.

Gultepe, I., and G. A. Isaac, Liquid water content and temperature relationship from aircraft observations and its applicability to GCMs, *J. Clim.*, *10*, 446–452, 1997.

Gultepe, I., D. O'C. Starr, A. J. Heymsfield, T. Uttal, T. P. Ackerman, and D. L. Westphal, Dynamical characteristics of cirrus clouds from aircraft and radar observations in micro and meso-γ scales, *J. Atmos. Sci.*, *52*, 4060–4078, 1995.

Gultepe, I., G. Isaak, D. Hudac, R. Nissen, and J. W. Strapp, Dynamical and microphysical characteristics of Arctic clouds during BASE, *J. Clim.*, *13*, 1225–1254, 2000.

Gultepe, I., G. A. Isaak, and S. G. Cober, Ice crystal number concentration versus temperature for climate studies, *Int. J. Climatol.*, *21*, 1281–1302, 2001.

Harrington, J. Y., M. P. Meyers, R. L. Walko, and W. R. Cotton, Parameterization of ice crystal conversion processes due to vapor deposition for mesoscale model using double-moment basis functions. part I: Basic formulation and parcel model results, *J. Atmos. Sci.*, *52*, 4344–4366, 1995.

Heckman, S. T., Numerical simulation of cirrus clouds: FIRE case study and sensitivity analysis, *Pap. 483*, 132 pp., Dep. of Atmos. Sci., Colo. State Univ., Fort Collins, 1991.

Heckman, S. T., and W. R. Cotton, Mesoscale numerical simulation of cirrus clouds: FIRE case study and sensitivity analysis, *Mon. Weather Rev.*, *121*, 2264–2284, 1993.

Heymsfield, A. J., Cirrus unicus generating cells and the evolution of cirriform clouds. part II: The structure and circulations of the cirrus uncinus generating head, *J. Atmos. Sci.*, *32*, 809–819, 1975.

Heymsfield, A. J., Precipitation development in stratiform ice clouds: A microphysical and dynamical study, *J. Atmos. Sci.*, *34*, 367–381, 1977.

Holroyd, E. W., A suggested origin of conical graupel, *J. Appl. Meteorol.*, *3*, 633–636, 1964.

Houze, R. A., Jr., *Cloud Dynamics*, Academic, San Diego, Calif., 1993.

Jakob, C., and J.-J. Morcrette, Sensitivity of the ECMWF model to the treatment of the ice phase, in *Workshop on Cloud Microphysics Parameterizations in Global Atmospheric Circulation Models, Kananaskis, Alberta, Canada, 23–25 May 1995*, *WMO/TD-713*, pp. 37–46, World Meteorol. Organ., Geneva, 1995.

Kelly, R. D., and G. Vali, An experimental study of the production of ice crystals by a twin-turboprop aircraft, *J. Appl. Meteorol.*, *30*, 217–226, 1991.

Kinne, S., T. P. Ackerman, A. J. Heymsfield, F. P. J. Valero, K. Sassen, and J. D. Spinhirne, Cirrus microphysics and radiative transfer: Cloud field study on 28 October 1986, *Mon. Weather Rev.*, *120*, 661–684, 1992.

Klemp, J. B., and R. B. Wilhelmson, The simulation of three-dimensional convective storm dynamics, *J. Atmos. Sci.*, *35*, 1070–1096, 1978a.

Klemp, J. B., and R. B. Wilhelmson, Simulations of right- and left-moving storms produced through storm splitting, *J. Atmos. Sci.*, *35*, 1097–1110, 1978b.

Krichak, S. O., and Z. Levin, On the cloud microphysical process during the November 2, 1994 hazardous storm in the southeastern Mediterranean as simulated with a mesoscale model, *Atmos. Res.*, *53*, 63–89, 2000.

Kuo, H. L., Further studies of the parameterization of the influence of cumulus convection on large-scale flow, *J. Atmos. Sci.*, *31*, 1232–1240, 1974.

Levkov, L., B. Rockel, H. Kapitza, and E. Raschke, 3D Mesoscale numerical studies of cirrus stratus clouds by their time and space evolution, *Beitr. Phys. Atmos.*, *65*, 35–58, 1992.

Liou, K.-N., Influence of cirrus clouds on weather and climate processes, *Mon. Weather Rev.*, *114*, 1167–1199, 1986.

Mahrer, Y., and R. A. Pielke, A numerical study of the airflow over irregular terrain, *Beitr. Phys. Atmos.*, *50*, 98–113, 1977.

Matrosov, S. Y., Theoretical study of radar polarization parameters obtained from cirrus clouds, *J. Atmos. Sci.*, *48*, 1062–1070, 1991.

Matrosov, S. Y., and R. A. Kropfli, Cirrus clouds studies with elliptically polarized Ka band radar signals: A suggested approach, *J. Atmos. Oceanic Technol.*, *10*(5), 684–692, 1993.

Matrosov, S. Y., B. W. Ott, R. A. Kropfli, and J. B. Snider, Retrieval of vertical profiles of cirrus cloud microphysical parameters from Doppler radar and infrared radiometer measurements, *J. Appl. Meteorol.*, *33*, 617–626, 1994.

McInnes, K. L., and J. A. Curry, Modelling the mean and turbulence structure of the summertime Arctic cloud boundary layer, *Boundary Layer Meteorol.*, *73*, 125–143, 1995.

Meyers, M. P., R. L. Walko, J. Y. Harrington, and W. R. Cotton, New RAMS cloud microphysics parameterization. part II: The two-moment scheme, *Atmos. Res.*, *45*, 3–39, 1997.

Miller, S. D., G. L. Stephens, C. K. Drummond, A. K. Heidinger, and P. T. Partain, A multisensor diagnostic satellite cloud property retrieval scheme, *J. Geophys. Res.*, *105*, 19,955–19,971, 2000.

Pelon, J., et al., Investigation of Cloud by Ground-based and Airborne Radar and Lidar (CARL), final report for the European Commission, DGXII, contract PL-970567, Brussels, 2001.

Pielke, R. A., et al., A comprehensive meteorological modeling system: RAMS, *Meteorol. Atmos. Phys.*, *49*, 69–91, 1992.

Platt, C. M. R., J. D. Spinhirne, and W. D. Hart, Optical and microphysical properties of a cold cirrus cloud: Evidence for regions of small particles, *J. Geophys. Res.*, *94*, 11,151–11,164, 1998.

Pruppacher, R. H., and J. D. Klett, *Microphysics of Clouds and Precipitation, Atmos. Oceanogr. Sci. Libr.*, vol. 18, 2nd ed., Kluwer Acad., Norwell, Mass., 1997.

Quante, M., H. Lemke, H. Flentje, P. Fransis, and J. Pelon, Boundaries and internal structure of mixed phase clouds as deduced from groud-based 95-GHz radar and airborne lidar measurements, *Phys. Chem. Earth, Part B: Hydrol. Oceans Atmos.*, *25*(10–12), 889–895, 2000.

Rangno, A. L., and P. V. Hobbs, Production of ice particles in clouds due to aircraft penetration, *J. Clim. Appl. Meteorol.*, *22*, 214–232, 1983.

Sassen, K., Aircraft-produced ice particles in a highly supercooled altocumulus cloud, *J. Appl. Meteorol.*, *30*, 765–775, 1991.

Sassen, K., and V. I. Khvorostyanov, Radar probing of cirrus and contrails: Insights from 2D model simulations, *Geophys. Res. Lett.*, *25*, 975–978, 1998.

Stackhouse, P. W., and G. L. Stephens, A theoretical and observational study of the radiative properties of cirrus: Results from FIRE 1986, *J. Atmos. Sci.*, *48*, 2044–2059, 1991.

Starr, D. O'C., and S. K. Cox, Cirrus clouds. part I: A cirrus cloud model, *J. Atmos. Sci.*, *42*, 2663–2681, 1985a.

Starr, D. O'C., and S. K. Cox, Cirrus clouds. part II: Numerical experiments on the formation and maintenance of cirrus, *J. Atmos. Sci.*, *42*, 2682–2694, 1985b.

Starr, D. O'C., et al., Comparison of cirrus clouds models: A project of the GEWEX Cloud System Study (GCSS) Working Group on Cirrus Cloud System, paper presented at 13th International Conference on Clouds and Precipitation (ICCP), Int. Assoc.of Meteorol. and Atmos. Sci., Reno, Nev., 14 –18 Aug. 2000.

Tremback, C. J., Numerical simulation of a mesoscale convective complex: Model development and numerical results, Ph.D. dissertation, Dep. of Atmos. Sci., Colo. State Univ., Fort Collins, 1990.

Tripoli, G. J., and W. R. Cotton, The Colorado State University three-dimensional cloud/mesoscale model-1982. part I: General theoretical framework and sensitivity experiments, *J. Rech. Atmos.*, *16*, 185–220, 1982.

Verlinde, J., P. J. Flatau, and W. R. Cotton, Analytical solutions to the collection growth equation: Comparison with approximate methods and application to cloud microphysics parameterization schemes, *J. Atmos. Sci.*, *47*, 2871–2880, 1990.

Walko, R. L., W. R. Cotton, M. P. Meyers, and J. Y. Harrington, New RAMS cloud microphysics parameterization. part I: The single moment scheme, *Atmos. Res.*, *38*, 29–62, 1995.

Woodley, W. L., T. L. Henderson, B. Vonnegut, G. Gordon, R. Breidenthal, and S. M. Holle, Aircraft-produced ice particles (APIPs) in supercooled clouds and the probable mechanism for their production, *J. Appl. Meteorol.*, *30*, 1469–1489, 1991.

Yuter, S. E., and R. A. Houze Jr., Three-dimensional kinematic and microphysical evolution of Florida cumulonimbus. part II: Frequency distributions of vertical velocity, reflectivity, and differential reflectivity, *Mon. Weather Rev.*, *123*, 941–963, 1995.

G. Kallos and E. Mavromatidis, School of Physics, Division of Applied Physics, University of Athens, University Campus, Building PHYS-V, Athens 15784, Greece. (kallos@mg.uoa.gr; imavr@mg.uoa.gr)